Chem Soc Rev

TUTORIAL REVIEW

View Article Online
View Journal

Cite this: DOI: 10.1039/c8cs00823j

Emerging two-dimensional monoelemental materials (Xenes) for biomedical applications

Wei Tao, †*[b] Na Kong,†[b] Xiaoyuan Ji,†[b] Yupeng Zhang, †[a] Amit Sharma, †[c] Jiang Ouyang,[b] Baowen Qi,[b] Junqing Wang,[b] Ni Xie,[a] Chulhun Kang,*[d] Han Zhang, *[a] Omid C. Farokhzad [b] and Jong Seung Kim *[c]

Received 2nd March 2019

DOI: 10.1039/c8cs00823j

rsc.li/chem-soc-rev

The emergence of novel two-dimensional (2D) monoelemental materials (Xenes) has shown remarkable potential for their applications in different fields of technology, as well as addressing new discoveries in fundamental science. Xenes (*e.g.*, borophene, silicene, germanene, stanene, phosphorene, arsenene, antimonene, bismuthene, and tellurene) are of particular interest because they are the most chemically tractable materials for synthetic exploration. Owing to their excellent physical, chemical, electronic and optical properties, Xenes have been regarded as promising agents for biosensors, bioimaging, therapeutic delivery, and theranostics, as well as in several other new bio-applications. In this tutorial review, we summarize their general properties including the classification of Xenes according to their bulk properties. The synthetic and modification methods of Xenes are also presented. Furthermore, the representative Xene nanoplatforms for various biomedical applications are highlighted. Finally, research progress, challenges, and perspectives for the future development of Xenes in biomedicines are discussed.

Key learning points

(1) Recent developments of Xenes, ranging from their structures, preparations, and physiochemical properties to biocompatibility.
(2) Design strategies of various Xene-based nanoplatforms.
(3) Xenes for various biomedical applications.
(4) Mechanisms and optimization approaches for improving Xenes' performances in biomedical applications.
(5) Current challenges and future developments of emerging Xenes in biomedicines.

1. Introduction

Two-dimensional (2D) materials, in general atomically thin sheets, have attracted extensive attention due to their superlative and unique properties.[1–3] Encouraged by the great success of graphene, a plethora of 2D materials have been developed and applied to various property-related applications such as energy, environmental science, catalysis, physics, and biomedicines. For example, transition metal dichalcogenides (TMDs), nitrides and carbonitrides (MXenes) and hexagonal boron nitride (h-BN), and their derivatives are all with sheet-like structures, which exhibit weak interlayer bonding and strong covalent in-plane bonding. With almost all of the atoms exposed on the surface after exfoliation (ultrathin form), the surface areas of these 2D materials are dramatically increased, which greatly improves their chemical and physical reactivities, and also affects a 2D wave function from quantum confinement effects. As a result, their ultrathin 2D structure can lead to unique photonic, catalytic, magnetic and electronic properties different from those of the bulk counterparts, endowing them with impressive advantages in the above-mentioned applications.

Most recently, emerging monoelemental 2D materials (Xenes) have attracted dramatically increasing attention,[3] especially after the great impacts due to the rapid development of phosphorene (also called black phosphorus) and borophene with unexpected excellent performance in nanotechnology applications,[4,5] which may address global societal challenges in electronics, energy,

[a] *Shenzhen Engineering Laboratory of Phosphorene and Optoelectronics and Key Laboratory of Optoelectronic Devices and Systems of Ministry of Education and Guangdong Province, Collaborative Innovation Center for Optoelectronic Science and Technology, and The First Affiliated Hospital, Shenzhen University, Shenzhen 518060, P. R. China. E-mail: hzhang@szu.edu.cn*
[b] *Center for Nanomedicine, Brigham and Women's Hospital, Harvard Medical School, Boston, MA 02115, USA. E-mail: wtao@bwh.harvard.edu*
[c] *Department of Chemistry, Korea University, Seoul 02841, Korea. E-mail: jongskim@korea.ac.kr*
[d] *The School of East-West Medical Science, Kyung Hee University, Yongin 17104, Korea. E-mail: kangch@khu.ac.kr*
† These authors contributed equally to this work.

environmentology, and healthcare. In particular, in biomedicines, owing to their excellent optical and electronic properties, Xenes have been regarded as promising biological theranostic agents for diagnosis [photoacoustic imaging (PAI),[6] photothermal imaging (PTI),[7] X-ray computed tomography (CT) imaging,[8] photoluminescence lifetime imaging (PLTI),[9] and fluorescence imaging (FI)[10]] and optical-therapeutic strategies [photodynamic therapy (PDT)[11] and photothermal therapy (PTT)[7]], highlighting their biomedical applications. The physical properties (*e.g.*, ultrahigh surface area-to-volume ratio) enable extensive surface interactions between Xenes and theranostic molecules (*e.g.*, therapeutic and fluorescent molecules), leading to an extremely high loading capacity,[10] which is impossible in traditional nanoparticle-based drug delivery platforms. In addition, rapid responses to external stimuli (*e.g.*, NIR laser irradiation and pH) could be achieved because of their ultrathin 2D structure, contributing to a triggered and/or controlled-release behaviour of loaded molecules (*i.e.*, release of multi-responsive therapeutics into the desired sites).[6] Further, the chemical properties (*e.g.*, tunable and versatile surface chemistry) of Xenes enable the attachment of various biological markers (*e.g.*, cellular growth factors, hydrogen peroxide (H_2O_2), DNA, *etc.*) for biosensing applications.[12] The range of analysis and sensitivity of Xene-based biosensors can be improved by their possible chemical functionalizations and tunable electrical properties.

The emerging 2D Xenes (*e.g.*, borophene, gallenene, silicene, germanene, stanene, phosphorene, arsenene, antimonene, bismuthene, tellurene, and selenene) have the potential to break through the limitations in the practical applications of other 2D materials.[2,5,13] For example, the low carrier mobility of TMDs hinders their use in various bio-sensing applications. Although MXenes and graphene have higher carrier mobilities, the limited bandgaps of MXenes and the zero bandgap of graphene prevent their applications in bioimaging, optical sensing, and field effect transistors (FETs). Despite the high electrical resistance that makes h-BN a good proton conductor, its biomedical applications are still limited by its insulating properties. Compared with these 2D materials, 2D Xenes (*e.g.*, phosphorene) have been demonstrated with tunable layer-dependent bandgaps, which holds great potential to bridge the space between h-BN (insulator), graphene (zero-bandgap), MXenes (limited bandgaps) and TMDs (large-bandgaps).[5] In this case, researchers can easily manipulate the strong interactions between Xenes and electromagnetic waves in a layer-dependent manner within the wavelength range from the ultraviolet (UV) to NIR region. This unique feature contributes to the excellent photoredox capability and large

Wei Tao received his PhD from Tsinghua University, and completed his postdoctoral fellowship in Prof. Omid Farokhzad's lab before his promotion to Instructor at Harvard Medical School (HMS) and Brigham and Women's Hospital (BWH).

Xiaoyuan Ji received his PhD from the Chinese Academy of Sciences. He is a Distinguished Researcher at Sun Yat-Sen University after his joint PhD training in the Center for Nanomedicine (CNM) at HMS/BWH.

Amit Sharma received his PhD from Guru Nanak Dev University, Amritsar, India, under the supervision of Prof. Kamaljit Singh. Thereafter, he joined Sphaera Pharma Pvt. Ltd, India, as a research scientist (2011–2014). In 2014, he joined Prof. Jong Seung Kim's research group as a research professor.

Baowen Qi received his PhD from the University of Montreal. Currently, he is a postdoctoral research fellow in the CNM at HMS/BWH.

Ni Xie is a Professor at the First Affiliated Hospital, Shenzhen University. Her research interests focus on the development, heterogeneity, metastasis and drug resistance mechanism of breast cancer, as well as the basic and clinical applications of molecular targets.

Han Zhang was born in Wuhan, China, in 1984. He received his PhD from Nanyang Technological University. He is currently a Professor and the Director of the Shenzhen Key Laboratory of 2D Materials and Devices, and the Shenzhen Engineering Laboratory of Phosphorene and Optoelectronics at Shenzhen University.

Na Kong is a clinician at the Second Affiliated Hospital Zhejiang University School of Medicine, and a Research Fellow at HMS/BWH. She received her MD from Zhejiang University.

Yupeng Zhang received his PhD from Wuhan University. From 2014 to 2017, he was a postdoctoral research fellow at Monash University. Currently, he is a Research Fellow at Shenzhen University.

Jiang Ouyang is a PhD candidate at Central South University, and a joint PhD student in the CNM at HMS/BWH.

Junqing Wang received his PhD from the Chinese University of Hong Kong. He is currently a postdoctoral research fellow in the CNM at HMS/BWH.

Chulhun Kang received his PhD from Iowa State University. Since 1997, he has been a faculty member at Kyung Hee University, where he is currently a Professor in the Department of Medical Science.

Omid Farokhzad is a Professor at HMS and a Physician-Scientist at BWH. He is the Founding Director of the CNM at BWH/HMS. He was a fellow of the National Academy of Inventors in 2018, and the American Institute of Medical and Biological Engineering (AIMBE) College of Fellows in 2012.

Jong Seung Kim was born in Daejon, Korea, in 1963. He received PhD from the Department of Chemistry and Biochemistry, Texas Tech University, and completed a one-year postdoctoral fellowship at the University of Houston. In 2007, he moved to the Department of Chemistry at Korea University in Seoul as a full professor.

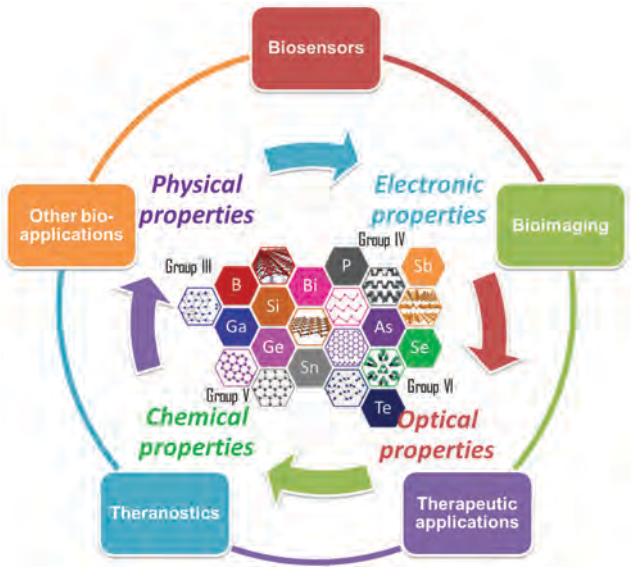

Fig. 1 An overview of the classification, properties, and biomedical applications of Xenes.

extinction coefficients of Xenes, making them excellent and tunable candidates in biosensors, bioimaging and optical-therapy strategies.[6,7,12,14] In addition, materials with simple elemental composition represent a unique advantage over other 2D multi-elemental materials due to the easier mechanisms of metabolism and degradability in biological systems. Moreover, Xenes are the most chemically tractable materials for synthetic exploration among the 2D material families.[15] The ultrathin 2D structure and its related physical properties are the major common characteristics of Xenes, while the atomic structures, elemental compositions, and interlayer forces are the distinguishing parts of each Xene that lead to different chemical, electronic and optical properties (introduced in Sections 2 and 3).

This tutorial review summarizes the significant progress of emerging 2D Xenes in various biomedical applications (Fig. 1). To start with, major types of Xenes and their general properties are introduced, followed by discussions on various Xene-based nanosystems that have been developed for different applications, including biosensors, bioimaging, therapeutic applications, and theranostics. As they are brand-new members in the 2D material families and many potential applications are still largely unexplored, we also shed some light on their most-recent novel bio-applications and hope these discussions will inspire future biomedical research on Xenes. We do not cover the biomedical applications of graphene since this has been extensively discussed elsewhere.[1] At last, we share our insights into the challenges and future developments.

2. Classification/types of Xenes

A brief summary of the general classification/types of emerging Xenes and their corresponding synthesis methods and characterization is presented in the following sections. The classification is organized by the periodic table group of Xenes as follows: Group III (*i.e.*, borophene and gallenene), Group IV (*i.e.*, silicene, germanene, stanene), Group V (*i.e.*, phosphorene, arsenene, antimonene, bismuthene), and finally Group VI (*i.e.*, selenene and tellurene). In addition, the predicted structure, synthesis, and characterization of different Xenes are briefly discussed. As shown in Fig. 2, the synthetic methods can be generally categorized as (i) top-down fabrication (*e.g.*, liquid-phase exfoliation, mechanical cleavage, and etching) and (ii) bottom-up synthesis (*e.g.*, chemical vapor deposition (CVD), physical vapor deposition (PVD), and wet-chemical solvothermal reaction).

2.1 Group III

Among the Group III family, the 2D forms of monoelemental boron (B) and gallium (Ga) materials, namely borophene and gallenene, have been successfully synthesized in experiments and are briefly discussed as follows.

2.1.1 Borophene (2D B). Because of the trivalent electronic configuration, B is one of the most chemically complex elements. By preventing the implementation of the octet rule, it results in an anomalous 'electron poor' bonding configuration, which further leads to electrons in B and/or its compounds being delocalized between three atoms (or more). The intrinsic geometric frustration between crystalline structures can be caused by this complexity in the pure bulk phase of B, generating 5–16 different polymorphs with highly complex unit cells.[16,17] The structures for several nanoscale B allotropes (*e.g.*, sheets and nanotubes) have been predicted by first-principles calculations. For the sake of simplicity, borophene is generally considered as the class of 2D B sheets.[4] Borophene has several unique characteristics. For instance, the structures of borophene are characterized by chemically-similar-structured anisotropy and polymorphism (Fig. 3a), which can provide an enhanced tunability of the properties.[4] For most structure models, borophene is believed to be metallic and can be identified as the lightest 2D metal, while exhibiting optical transparency and mechanical compliance at the same time. The metallic property of borophene is quite different from semimetals (*e.g.*, silicene) and semiconductors (*e.g.*, phosphorene). Neither conventional nor synthetic 2D materials have such combined properties, thus highlighting the uniqueness of borophene. Borophene is also expected to have relatively high-temperature superconductivity as the transition temperatures are predicted to be 10–20 K. Experimental synthesis of borophene has been successfully achieved (Fig. 3b), and the reported methods include PVD, mechanical cleavage, etching, and liquid-phase exfoliation.[4,14]

2.1.2 Gallenene (2D Ga). Ga, a metal which exists as a liquid at room temperature, has a rich low-temperature phase diagram. Optical low-power-consumption, phase-change memories have been demonstrated with the chemical stability of Ga. The theoretical aspects of the structure of gallenene are presented in Fig. 3c; monolayers of Ga along 010 (b_{010}) and along 100 (a_{100}) from α-Ga were extracted and then relaxed in order to establish an atomically thin layer of gallenene.[18] Followed by the complete relaxation, b_{010} retains its former structure, while a_{100} changes into a honeycomb structure. The relaxed gallenene b_{010} has a lower symmetry and resembles a form of zigzag rhombic lattice. Different from gallenene a_{100}, two Ga dimers are separated (along the vertical direction) by 1.32 Å in the quasi-2D multidecker structure of

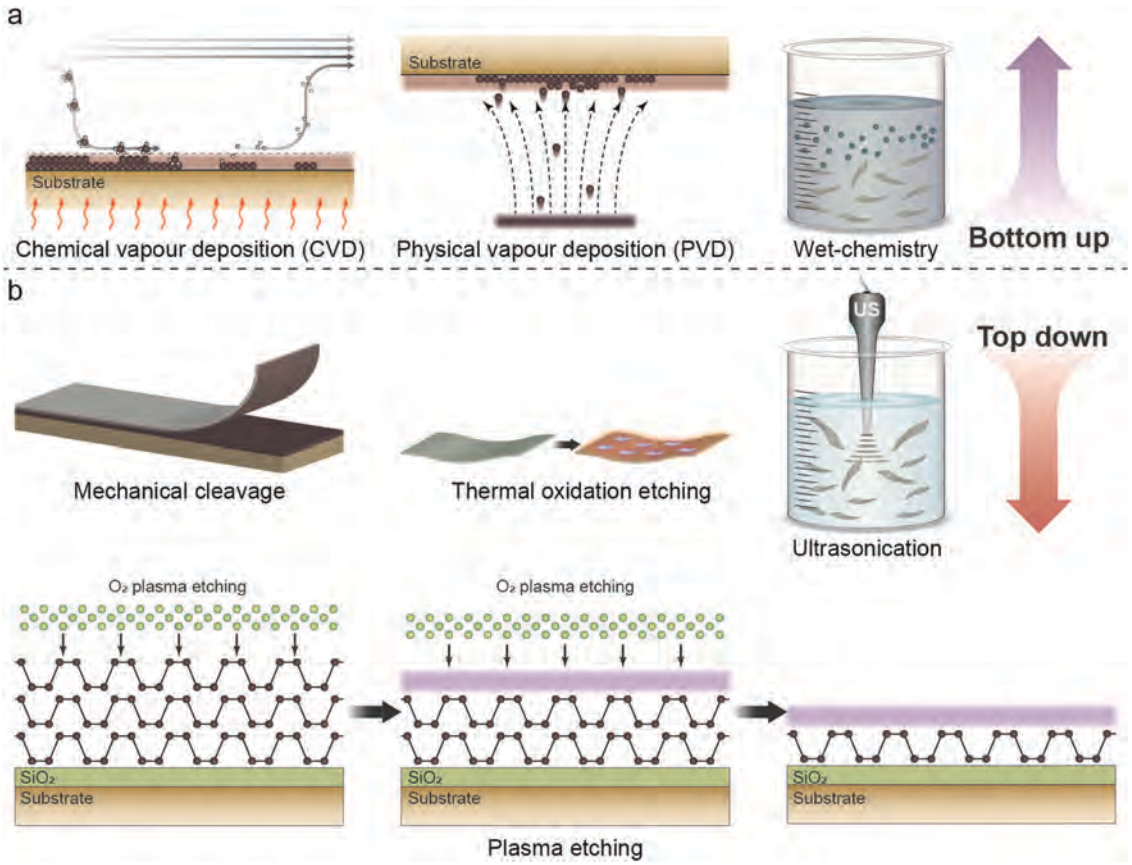

Fig. 2 Schematic illustration of the synthesis methods of Xenes: (a) top-down fabrication and (b) bottom-up synthesis.

gallenene b_{010}. Other Xenes including silicene, germanene, stanene, and phosphorene can also have such buckling. Experimental gallenene has been obtained very recently (Fig. 3d), and the reported methods include PVD and solid–melt exfoliation.[18,19]

2.2 Group IV

Derived from silicon (Si), germanium (Ge), and tin (Sn) in the Group IV family, the 2D Group-IV monolayer materials are named silicene, gallenene, and stanene, respectively. Although in the same Group IV family with graphene, heavier members like silicene, gallenene, and stanene do not favour sp^2 hybridization. This leads to a similar buckled honeycomb structure, which has a mixed degree of sp^2–sp^3 character. In addition, it is expected that the heavier Group IV elements, due to their enhanced spin–orbit coupling, can exhibit topologically non-trivial electronic states.[20]

2.2.1 Silicene (2D Si). Although the Group IV family members have commonalities, Si is quite different from carbon (C). For example, instead of the sp^2-hybridized C atoms in bulk graphite, Si features sp^3-hybridized tetrahedrally bonded atoms in the bulk form. As indicated by first-principles calculations, the monolayer silicene, which possesses a honeycomb crystal structure, is stably combined in a non-planar buckled configuration (Fig. 4a). It is predicted that silicene has graphene-like Dirac fermions and shows semi-metallic characteristics. Compared with graphene, silicene exhibits enhanced spin–orbit coupling effects and has a lower symmetry, buckled honeycomb structure. Theoretically, these differences indicate that silicene could host topologically non-trivial electronic states, gate-tunable bandgaps, and spin-polarized edge states. All of these properties enable the application of silicene-based devices in tunable transistors or photodetectors.[15] Experimental synthesis of silicene has been successfully obtained (Fig. 4b), and the reported methods include PVD and chemical exfoliation.[21,22]

2.2.2 Germanene (2D Ge). As the Ge analogue of silicene (also identified as the "brother" of silicene), germanene has the same buckled honeycomb structure (Fig. 4a). The first prediction of germanene, which originates from first-principles total-energy calculations, suggests that the Ge atoms tend to form a corrugated aromatic stage and construct a corrugated 2D layer-structure. Due to its similar properties to silicene, germanene is briefly discussed here. The larger atomic number of Ge (*i.e.*, heavier element) is the primary difference, which results in an enhanced spin–orbit coupling. As a result, germanene possesses stronger topological insulator characteristics than those of silicene. Experimental germanene (Fig. 4c) has been developed through different methods, such as mechanical cleavage and PVD.[2,23]

2.2.3 Stanene (2D Sn). The tin (also called stannum) element locates in a deeper position of Group IV in the periodic table. A similar buckled honeycomb lattice structure was recognized through structural predictions (Fig. 4a). As in Si and Ge, some overlap between π and σ orbitals can be induced by two-level

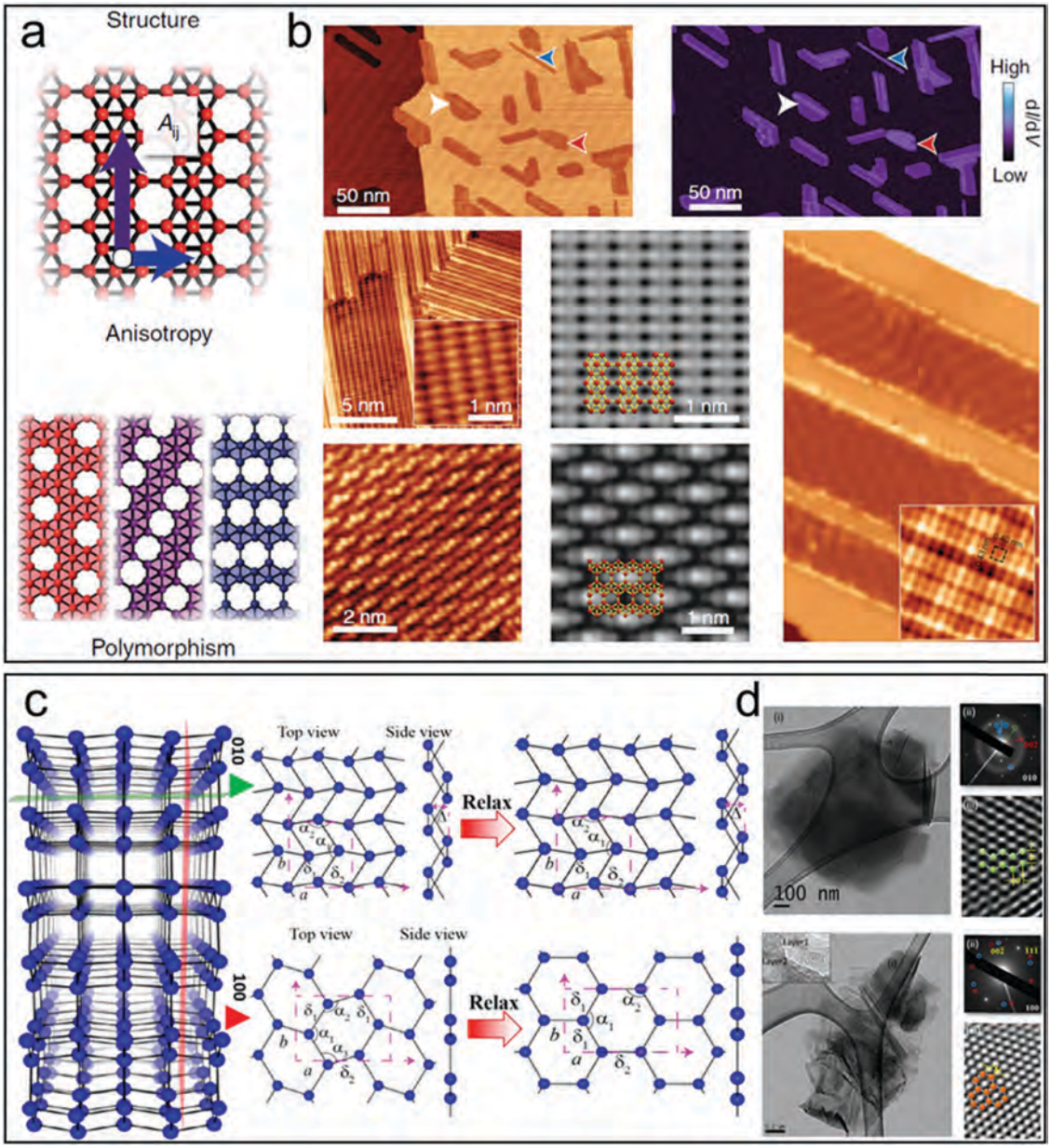

Fig. 3 Xenes in Group III (borophene and gallenene). (a) Structure and (b) experimental morphological (STM) images of borophene (PVD preparation). Reprinted with permission from ref. 4. Copyright 2018 Macmillan Publishers Limited, part of Springer Nature. (c) Structure and (d) experimental morphological (TEM) images of gallenene (solid–melt exfoliation preparation). Reprinted with permission from ref. 18. Copyright 2018 American Association for the Advancement of Science.

buckling, which makes the π–π bonding within the atomic plane relatively more stable. Similarly, as Sn is the heaviest (atomic mass) element among C, Si and Ge, its spin–orbit coupling is the strongest. A divergence from the Dirac fermion behaviour typical of graphene would be generated by introducing the spin–orbit coupling effects into the band structure calculations. This would further cause an opening of a bandgap (~0.1 eV) bridged (at the material edges) by a topologically nontrivial state.[15] Due to its special electronic structure, stanene, known as a new "cousin" of graphene,[24] is promising as a topological insulator. Stanene has been successfully prepared in experiments through PVD (Fig. 4d).[24]

2.3 Group V

Among the Group V family, the 2D forms of monoelemental phosphorus (P), arsenic (As), antimony (Sb) and bismuth (Bi) materials, namely phosphorene, arsenene, antimonene and bismuthene, respectively, have been experimentally prepared, and are briefly discussed in this section.

2.3.1 Phosphorene (2D BP). The allotropes of phosphorus (P) include gaseous phosphorus (GP), black phosphorus (BP), blue phosphorus (BuP), white phosphorus (WP), violet phosphorus (VP), and red phosphorus (RP). WP, also named yellow phosphorus, is the most toxic allotrope of P (therefore maybe

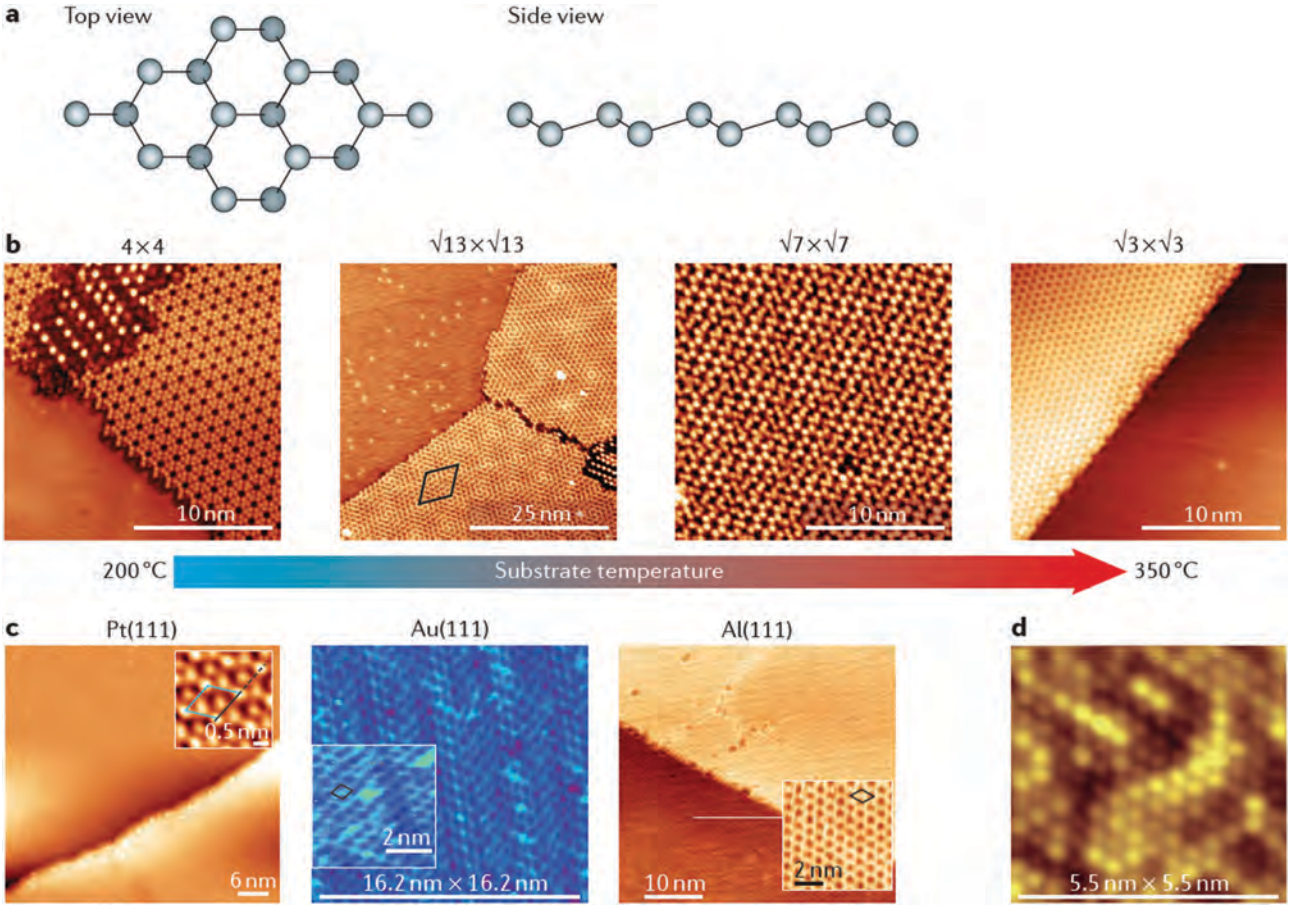

Fig. 4 Xenes in Group IV (silicene, germanene, and stanene). (a) Structures for freestanding silicene, germanene, and stanene. (b) Experimental morphological (STM) images of silicene (Si–Si bond length: 0.2233 nm; vertical displacement: 0.045 nm). (c) Experimental morphological (STM) images of germanene (Ge–Ge bond length: 0.2344 nm; vertical displacement: 0.0069 nm). (d) Experimental morphological (STM) images of stanene (Sn–Sn bond length: 0.2698 nm; vertical displacement: 0.0085 nm). Silicene, germanene, and stanene were prepared *via* PVD. Reprinted with permission from ref. 15. Copyright 2017 Macmillan Publishers Limited, part of Springer Nature.

not suitable for biomedical applications) and possesses a tetrahedral P_4 structure, where each P atom is bound to three other P atoms by a single bond. RP can be formed by heating WP to 250 °C and has a polymeric chain-like structure. VP with a monoclinic structure can be produced by day-long annealing of RP over 550 °C. GP, also called diphosphorus (P_2), is the gaseous allotropic form of P and generated by the thermolysis (cracking) of P_4 (WP) at 1100 K. Meanwhile, BuP is another stable phase of P and has a hexagonal structure. More detailed information regarding the structures and properties of these allotropes has been provided elsewhere.[25] As the most thermodynamically stable allotropic form among them, BP is also the most extensively studied one at present. We should state that the phosphorene discussed in this review only refers to 2D BP. As shown in Fig. 5a (α phase), BP has a layered orthorhombic structure with space group *Cmca*, which contains parallel-puckered and double-floor atomic layers. From the 3p and 3s orbitals, each P atom has five valence electrons within an individual atomic layer, and hybridizes to develop covalent bonds (n = 3) with neighboring P atoms. One of the three covalent bonds is nearly perpendicular to the atomic plane, which connects P atoms from the lower and upper layers, while the other two are parallel to the atomic plane. BP is able to transform into another semi-metallic β phase (under ~5 GPa) with space group $R\bar{3}m$. The β phase is a double-layered, rhombohedral structure that consists of plentiful ruffled, interlocked, and six-membered rings. Although the first study on BP could be dated back to over one hundred years ago, BP, which has been extensively reported in various applications, could be considered as the hottest Xene after graphene.[5] Because of the tremendous studies on BP, the experimental methods for the synthesis of phosphorene are the most among the discussed Xenes (Fig. 5b). The recently reported methods include mechanical cleavage, liquid-phase exfoliation, etching, CVD, PVD, and wet-chemistry.[5,10,26]

2.3.2 Arsenene (2D As). Gray, yellow and black As are three common allotropes of arsenene. With a layered rhombohedral structure (β phase, space group $R\bar{3}m$), gray As is the most typical as well as the most stable form among the three allotropes. Notably, the β-phase gray As is a natural layer crystal that has been known for over 1000 years. Gray As, with bands close to the L and T points which are partly overlapped, is a semi-metal material.

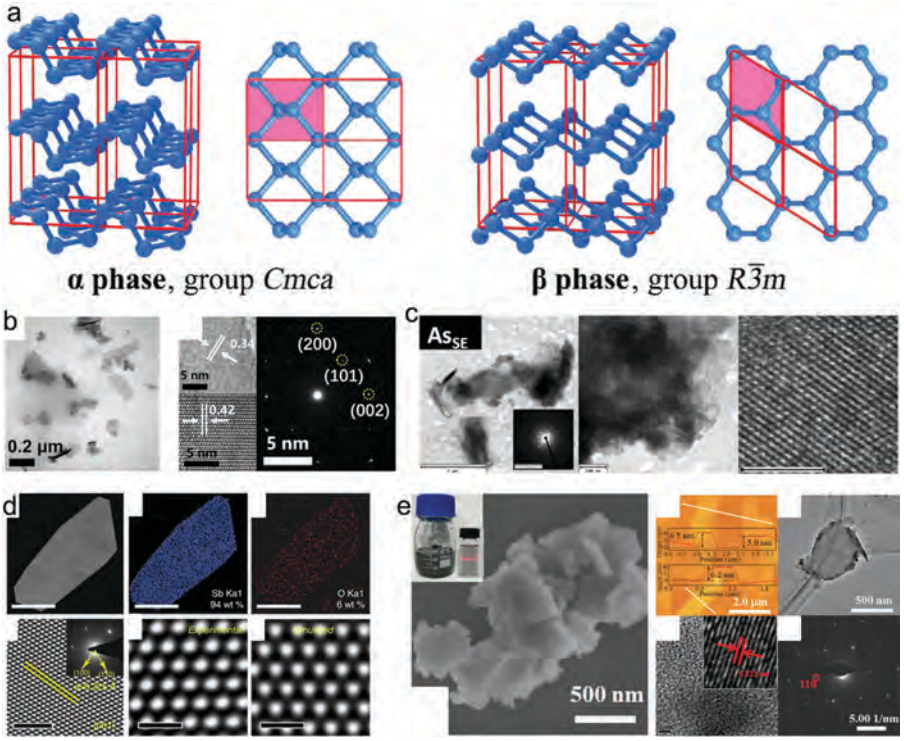

Fig. 5 Xenes in Group V (phosphorene, arsenene, antimonene, and bismuthene). (a) Structures for phosphorene (α and β phases), arsenene (α and β phases), antimonene (β phase), and bismuthene (β phase). Reprinted with permission from ref. 13. Copyright 2018 Royal Society of Chemistry. (b) Experimental morphological (TEM) images of phosphorene (liquid-phase exfoliation preparation). Reprinted with permission from ref. 26. Copyright 2018 National Academy of Sciences. (c) Experimental morphological (TEM) images of arsenene (liquid-phased exfoliation preparation). Reprinted with permission from ref. 27. Copyright 2017 Wiley. (d) Experimental morphological (TEM) images of antimonene (PVD preparation). Reprinted with permission from ref. 28. Copyright 2016 Macmillan Publishers Limited, part of Springer Nature. (e) Experimental morphological (SEM and TEM) images of bismuthene (liquid-phased exfoliation preparation). Reprinted with permission from ref. 31. Copyright 2018 Royal Society of Chemistry.

The layered orthorhombic structure (α phase, space group *Cmca*), which is similar to that of BP, could be obtained upon heating As to ~370 K. With a bandgap of ~0.3 eV, the α-phase orthorhombic As can be a narrow-gap semiconductor. Arsenene has been successfully synthesized through mechanical cleavage and liquid-phase exfoliation (Fig. 5c).[13,27]

2.3.3 Antimonene (2D Sb). Bulk Sb also has three common allotropes (*e.g.*, gray, black, and explosive Sb). Gray Sb, which has the same rhombohedral structure (β phase, space group $R\bar{3}m$) as gray As, is the most stable among all these allotropes. Bulk gray Sb has typical semimetal characteristics, like bulk gray As. Upon rapid cooling of Sb vapor, black Sb could be effectively formed. However, black Sb is highly chemically active in an atmospheric environment. Even under vacuum, it can easily transform into more stable crystalline gray Sb at ~373 K. Under heating or mechanical stress, explosive Sb could also transform fiercely into gray Sb.[13] A semiconductor behaviour (theoretical bandgaps up to 2.28 eV) could be achieved after exfoliating Sb down into antimonene. The experimental fabrication of antimonene has been successfully achieved (Fig. 5d) under the guidance of fast development in theoretical calculations and the experimental methods include mechanical cleavage, PVD, and liquid-phase exfoliation.[6,7,13,28]

2.3.4 Bismuthene (2D Bi). Bulk Bi has only one stable form, which is a rhombohedral structure (β phase, space group $R\bar{3}m$) like Sb. Bi, with a naturally layered structure, is metallic and the heaviest among the Group V elements discussed here. Thanks to its large atomic mass and concomitantly strong spin–orbit coupling, Bi is identified as a common component in topologically non-trivial systems. Its 2D form, bismuthene, has been predicted to possess the ability to act as a 2D topological insulator. However, the topological characteristics of a different buckled honeycomb structure are still under debate.[15] Therefore, it is vital to measure the electrical transport properties of isolated buckled honeycomb bismuthene layers for the better understanding of Bi's electronic properties, with the purpose of quantifying the influence of spatial confinement on the electrical properties in depth. Among them, scanning tunneling microscopy (STM) and high-resolution electron diffraction microscopy are the most widely techniques for measuring the electrical transport properties of bismuthene films,[29] which further corroborated their correlation with the films' thickness. The spin-split free-electron system is another recently developed technique to explore the electrical transport properties of bismuthene films by applying electrical fields *via* a four-tip STM using a magnetic probe. These experimental data were also correlated with theoretical analysis based on the Rashba effect.[30] Different methods reported to experimentally synthesize bismuthene (Fig. 5e) are mechanical cleavage, PVD, and liquid-phase exfoliation.[2,13,31]

2.4 Group VI

Derived from selenium (Se) and tellurium (Te) in the Group IV family, the 2D Group-IV monolayer materials are named selenene and tellurene, respectively. Different from the aforementioned elements, Group VI elements always possess 3D bulk structures, which consist of 0D atomic rings or 1D atomic chains with two-fold coordination bonding, under ambient conditions. The 2D forms of Se and Te have been experimentally prepared, and are briefly discussed in this section.

2.4.1 Selenene (2D Se). By utilizing density functional theory (DFT) calculations within the generalized gradient approximation (GGA), the structures for Se are reported to be composed of 0D atomic rings (Fig. 6a(i)) or 1D helical atomic chains (Fig. 6a(ii)).[32] The Se–Se distance within the rings or chains is 2.4 Å, while that between atoms in nearby chains or rings is over 3.1 Å. Therefore, van der Waals interactions dominate the interaction between nearby atomic chains or rings. The 2D atomic layered structure for Se (*i.e.*, selenene) has been predicted by first principles calculations.[32] As shown in Fig. 6a(iii), Se atoms are arranged in a buckled square lattice (*i.e.*, two Se atoms per unit cell) within this structure. The structure is a bit similar to those of the Group IV Xenes with chair-like puckering (*e.g.*, the X atom in the center of the unit cell leans toward one corner), but the unit cell is twisted into a square. Strong covalent bonds connect all of the Se atoms in the layer structure. Se has been identified as a potential anti-angiogenic or anti-metastatic agent that can be used for cancer chemotherapy. In addition, a recent study also reported the promising application of Se-based materials as radiosensitizers for effective cancer radiotherapy. Because of the special properties of the chemical element Se, the future development of Se is worth expecting in the area of combinational therapy for cancer. 2D Se (selenene) has been experimentally obtained with the PVD method (Fig. 6b).[33]

2.4.2 Tellurene (2D Te). As shown in Fig. 6c, a characteristic chiral-chain crystal lattice can be observed in tellurene, where Te atoms are stacked together between individual helical chains by van der Waals type bonds, and spiral around axes parallel toward the [0001] direction at both the corners and center of the hexagonal unit cell.[34] The Te atom is covalently bonded with the adjacent Te atoms on the same chain. Because of its spin–orbit coupling, bulk Te has high hole mobilities and small effective masses. A slightly indirect bandgap (~0.35 eV) in the infrared

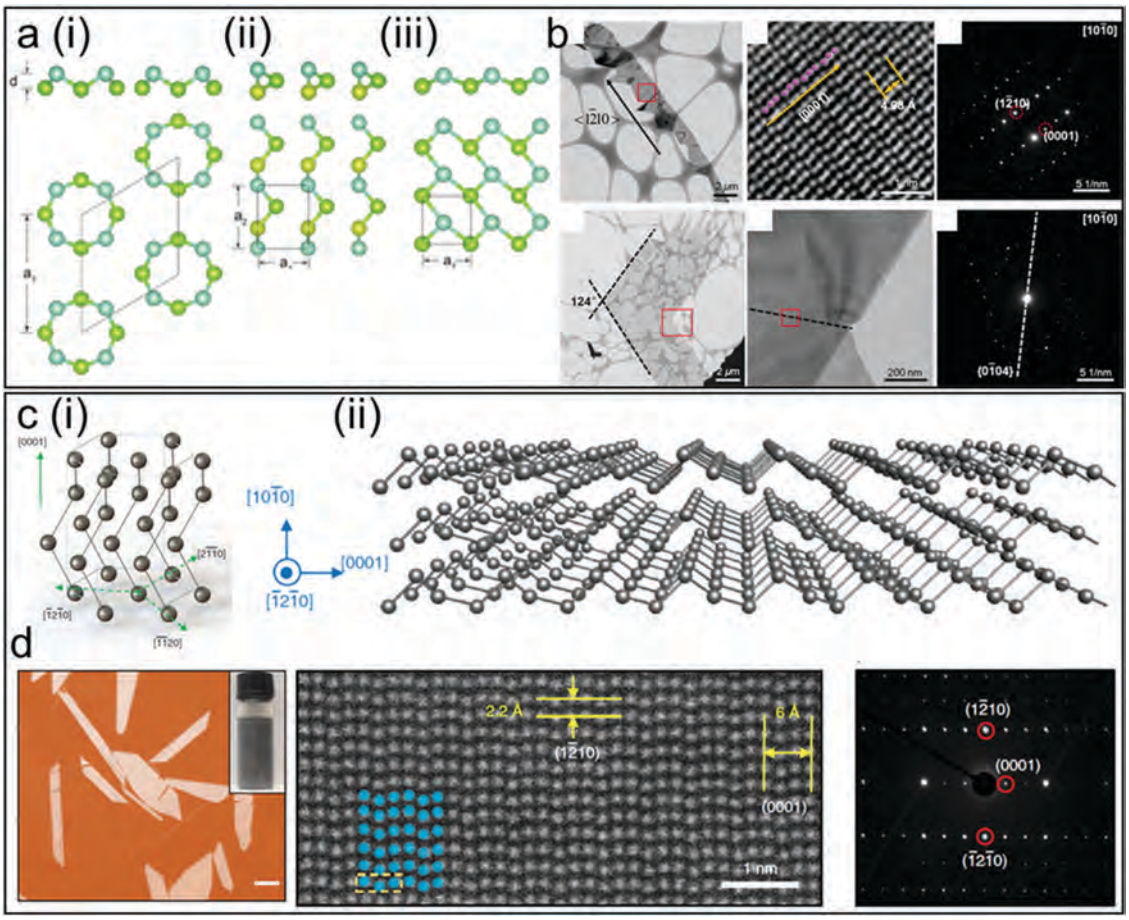

Fig. 6 Xenes in Group VI (selenene and tellurene). (a) Structures for Se and selenene. Reprinted with permission from ref. 26. Copyright 2017 IOP Publishing Ltd. (b) Experimental morphological (TEM) images of selenene (PVD preparation). Reprinted with permission from ref. 32. Copyright 2017 American Chemical Society. (c) Structures for Te and tellurene. (d) Experimental morphological (optical and STEM) images of tellurene (wet-chemistry preparation). Reprinted with permission from ref. 34. Copyright 2018 Macmillan Publishers Limited, part of Springer Nature.

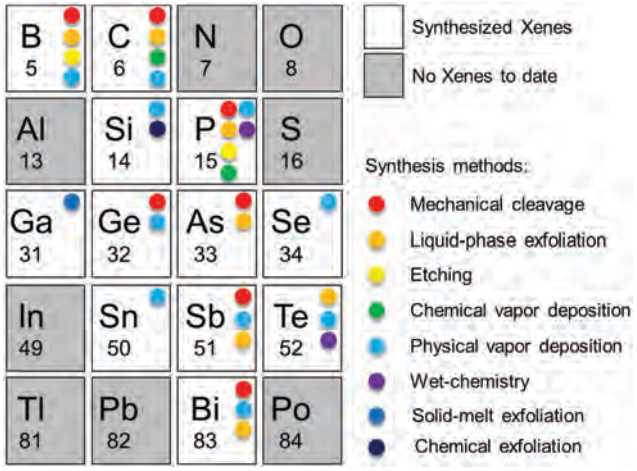

Fig. 7 Elements predicted to form emerging Xenes and their known synthesis methods. Elements shown in grey have not been predicted or have been experimentally verified to form Xenes.

regime could be induced by the anti-bonding and lone-pair orbitals in bulk Te. According to first-principles calculations, the indirect feature could be more prominent when its thickness is reduced.[34] A buckled square structure of Te (named square tellurene), similar to selenene shown in Fig. 6a(iii), could also appear as the second lowest energy structure.[33] Only 0.06 eV per atom of energy difference could be found between the two tellurenes in the freestanding form.[32] Such a cohesive energy difference could be easily compensated for by the adsorption energy difference when using appropriate substrates to grow tellurene. Te is a semiconductor, which can generate active electrons and vacancies (under certain irradiation conditions), which react with the ambient environment, and induce oxidative stress. This unique property enables tellurene to be adopted for bio-catalysis and PDT in the future development of biomedical fields. Recent studies have reported different methods for the synthesis of tellurene in experiments, such as wet-chemistry,[34] liquid-phase exfoliation,[11] and PVD.[35]

The general classification/types of emerging Xenes and their corresponding synthesis methods are presented in Fig. 7. For more detailed discussions regarding the predicted structure, synthesis, and characterization of different emerging Xenes, the reader can also refer to other excellent reviews and perspectives.[2–4,13]

3. General properties of Xenes

Recently, various emerging Xenes have been investigated and demonstrated to exhibit excellent physical, chemical, electronic, and optical properties. These properties are both material-dependent and versatile, favoring the specific applications of the emerging Xenes. In addition, there are also commonalities between different Xenes. We briefly highlight these properties in this section.

3.1 Physical properties

The physical properties of Xenes, *i.e.*, structural properties, are among the most unique properties compared to other non-2D materials. For example, due to the ultrahigh surface area-to-volume ratios of Xenes, extensive surface interactions between Xenes and functional molecules (*e.g.*, therapeutic, diagnostic, and theranostic molecules) could be generated, which could lead to an extremely high loading capacity of these molecules.[6,10,14] Compared with conventional nanoparticle-based drug delivery platforms, which usually have 10–30% (w/w%) of drug loading at most,[10] this advantage is quite inviting. Moreover, benefitting from their ultrathin 2D structure, the emerging Xenes could exhibit rapid responses to external stimuli (*e.g.*, NIR laser irradiation and pH change). This advantage could generate a spatiotemporally controlled-release behaviour of the loaded molecules (*i.e.*, release of multi-responsive therapeutics) in the desired or disease sites,[6] further highlighting their applications in drug delivery systems. However, we also need to recognize that such physical properties can also be found in other 2D nanomaterials such as MXenes and TMDs. In addition, different Xenes in different periodic table groups have differentiated bulk structures (as discussed in our above sections), which may provide more choices of synthetic methods for the emerging Xenes.

3.2 Chemical properties

The chemical properties of Xenes, especially their stability under ambient conditions and their degradability in a biological system, are critical characteristics for their application in biomedicine. Although some Xenes show poor stability in air or water, non-covalent, inorganic or covalent functionalization could be applied to provide enhanced stability and tunable properties. Their poor stability may be a unique advantage specific for biomedical applications since it means easy degradability and metabolism. Besides, the mechanisms of metabolism and degradability of Xenes (*e.g.*, phosphorene) in biological systems have also been explored,[36] which makes them interesting for biomedical applications. Moreover, macro elements (*e.g.*, P), trace elements (*e.g.*, Si and B), and ultra-trace elements (*e.g.*, Se, As, Sn, Ga, Ge, Bi, and Sb) have also been identified as essential for human health and life. These properties may provide the possibility of use of these monoelemental-based Xenes for safe biomedical applications. In addition, the tunable and versatile surface chemistry of Xenes makes the attachment of biological markers possible, which could be used as biosensors.[5,37] By further chemical functionalization, the range of analysis and the sensitivity of Xene-based biosensors can be tuned and versatile, which makes Xenes good candidates for biosensing applications.

3.3 Electronic properties

Different from those of other 2D materials, the electronic properties of Xenes are very distinctive, which are strongly determined by the nature of the X element. Theoretical and experimental studies indicated that the emerging Xenes may show metallic or semiconductor-like properties by changing their thickness, while some bulk forms of Xenes may also present insulating properties (*e.g.*, Bi). As introduced in the above sections, the metallic, semiconductor-like, or insulator-like properties could also be achieved by simply adopting different kinds of Xenes.

For example, borophene is metallic, silicene is semi-metallic, and stanene is insulator-like. In addition, a direct and tunable bandgap could be found in some Xenes (*e.g.*, phosphorene),[5] and this property is determined by the number of layers. Because of the surface terminations and different extents of defects, the synthetic methods could also change the electronic properties of Xenes. In general, more defects could cause lower conductivity due to the destructed structure for free movement of electrons. By element doping, such kinds of defects can be introduced into the emerging Xenes. The conductivity changes of Xenes can be utilized for detecting signal molecules (*e.g.*, gases, oxides and reducing agents). The attachment of these molecules on the surfaces of Xenes could lead to changes in electronic signals, which is promising for the ultrasensitive detection of biomarkers. Under certain stimuli (*e.g.*, light excitation), semiconductor-like Xenes are able to generate active electrons and vacancies, which can further react with the ambient environment and impose oxidative stress. Such a feature is an essential process of catalysis and/or reactive oxygen species (ROS) generation, which could further benefit their applications in bio-catalysis and PDT. In addition, the conductivity of Xenes could be accurately measured by monitoring the current changes between the electrically excited objects after binding with bio-species. The changes in the local charge field trigger a signal accumulation reflected by a change in its conductivity. The advantage of Xenes used in biosensors is that the cross-sectional area is on an identical spatial scale to the charge field for the bound biomolecules nearby, which functions as a minimal spatially confined target to sense the electrical alteration as a function of the measured conductivity.

3.4 Optical properties

The optical properties (*e.g.*, light absorption and conversion) of Xenes are critical and important for their applications in the biomedical field. With a broad range of absorption spectra from UV-visible to NIR, the strong absorption properties of Xenes have great potential for their applications in PTT and PAI in the biological window.[6,14] It has been well-demonstrated that the emerging Xenes have excellent photothermal conversion efficiency (*e.g.*, approaching 50%).[7,14] Additionally, Xenes could also be used as photosensitizers to effectively produce ROS, which could selectively kill both bacteria and cancer cells, thus making Xenes great candidates for PDT.[11] Some Xenes (*e.g.*, phosphorene) also have a strong localized surface plasmon resonance (LSPR) effect, which can make them promising substrates for surface-enhanced Raman spectroscopy (SERS).[5] Together with their inherent biocompatibility, such an ability makes Xenes promising for high-resolution bioimaging and Raman scattering-based sensing applications. Moreover, the emission ability of Xenes is another valuable property, which can be utilized for PLTI under excitations at particular wavelengths.[9] Such luminescence properties could benefit bioimaging and optical-based biosensing. These optical properties can be tuned by developing various Xenes with different compositions, sizes, thicknesses and surface modifications, thus facilitating their utilization in different biomedical fields.

4. Biomedical applications of Xenes

Because of their outstanding physical, chemical, electronic and optical properties, 2D Xenes have been explored in a number of applications in biomedical fields including biosensors, bioimaging, therapeutics, theranostics, and other novel bio-applications (*e.g.*, antimicrobials and neuroprotective nanomedicines) (Fig. 1). The various adopted strategies in this field are discussed below.

4.1 Design and surface functionalization of Xenes for biomedical applications

Appropriate surface modification/functionalization enables enhanced biomedical performance (*e.g.*, circulation, loading capacity, targeting ability, biocompatibility). Compared to their pristine forms, surface functionalized 2D Xene nanomaterials exhibit fundamentally enhanced dispersion stability, surface reactivity, and *in vivo* degradation kinetics, achieving maximal biological outcomes and minimal toxic responses. In this regard, various designs and surface modifications have been developed to improve the potential of emerging Xenes for further biomedical applications through physical absorption or electrostatic attraction. A summary of the design and surface modifications of Xenes is provided in this section, such as polyethylene glycol (PEG) coating, poly(vinylpyrrolidone) (PVP) protection, poly(lactic-*co*-glycolic acid) (PLGA) encapsulation, and targeting linker functionalization.

As an arising star in the Xene family, silicene (2D Si) is a silicon analogue of graphene and is widely utilized in various silicon-based biosensor preparations. However, pristine silicene is unstable and prone to aggregate in physiological solutions, such as cell-culture media or serum, thus limiting its applications in the biomedical realm. Fortunately, silicene tends to be surface modified easily as compared to graphene, which is the result of the sp^3 hybridization of silicene instead of the sp^2 hybridization of graphene.[38] The use of covalent chemistry serves as an effective regulator for tailoring the properties, such as tuning the electronic properties of silicene with the surface adsorption of alkali metal (Fig. 8a).[39]

Regarding the therapeutic and theranostic applications of the emerging Xenes, their colloidal stability and biocompatibility are the premise for *in vivo* studies. PEG coating (*i.e.*, PEGylation) is one of the most commonly used strategies (Fig. 8b). For example, Ji *et al.* modified exfoliated borophene (2D B) nanosheets using PEG-NH_2 with a molecular weight of 2000.[14] Due to the abundant BO_3^{3-} on the surfaces of the nanosheets, positively charged PEG-NH_2 can be coated on the surface of borophene *via* strong electrostatic adsorption. The extent of the PEG layer in PEGylated borophene was determined to be $\approx$33.6% (w/w) in total with inductively coupled plasma-atomic emission spectrometry (ICP-AES). This amount of PEG is enough to realise borophene with remarkably better stability and dispersibility compared to bare borophene, and also negligible agglomeration was observed in both phosphate buffer saline (PBS) and cell culture medium up to 24 h of incubation. In addition, for other kinds of Xenes with different surface properties (majorly depending on the difference in exfoliation methods), different

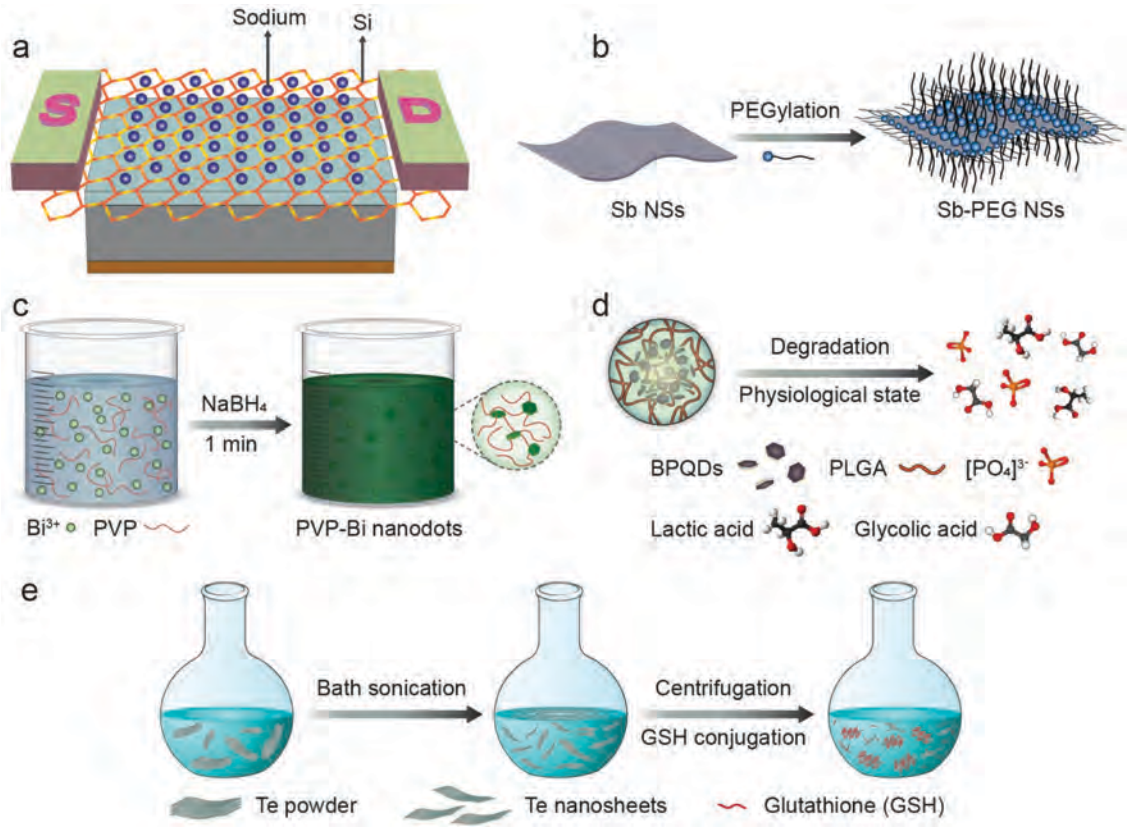

Fig. 8 Examples of the surface functionalization strategy of emerging Xenes for biomedical applications. (a) Surface adsorption of alkali metal for silicene; (b) PEGylation of antimonene; (c) PVP-coating of bismuthene; (d) encapsulation of phosphorene in PLGA polymer; and (e) GSH modification of tellurene.

strategies should be considered. For instance, hydrophobic 1,2-distearoyl-*sn-glycero*-3-phosphoethanolamine-*N*-[methoxy(polyethylene glycol)] (DSPE-PEG) with a molecular weight of 3000 was chosen for the surface modification of antimonene (2D Sb) nanosheets exfoliated from ethanol.[6] Because of their highly hydrophobic surface, the lipid part (DSPE) of DSPE-PEG could interact with antimonene through hydrophobic interactions to improve their stability and dispersity. Lin and co-workers also reported a method of using glutathione (GSH) to modify the surfaces of tellurene (2D Te) nanosheets exfoliated from dimethylformamide (DMF) to improve their stability and avoid oxidation (Fig. 8e).[11]

PVP can also be used to effectively protect the emerging Xenes and improve their stability under physiological conditions. For example, Lei *et al.* provided an ultra-facile organic solvent strategy (Fig. 8c) for developing PVP-protected bismuth (2D Bi) nanodots and applied them as monoelemental theranostic nanoplatforms for dual-modal CT/PTI-guided PTT.[8] The distinct advantages of this unique method include the following: (i) it involves rapid one-step synthesis of PVP-protected bismuthene nanodots, improving the efficiency of synthesis and avoiding further modification of the nanodots, and (ii) it is conducive to mass production and nontoxic.

For ultrasmall Xene quantum dots (QDs), US Food and Drug Administration (FDA)-approved polymer PLGA can also be used to encapsulate the developed Xene QDs for improved stability and *in vivo* performance in therapeutic and theranostic applications. For example, after being prepared by a combined liquid-phase exfoliation method [both probe and bath sonication in *N*-methyl-2-pyrrolidone (NMP)], the synthesized phosphorene (2D BP) QDs were loaded into PLGA by an emulsion method (Fig. 8d).[36] The prepared BPQDs could be easily degraded in air and thus may have the problem of generating a persistently good photothermal effect. By encapsulating the BPQDs into PLGA nanospheres, the solid PLGA core could protect the BPQDs from environmental oxygen and water and simultaneously tune the degradation rate (increased from days to weeks). Therefore, the photothermal stability can be enhanced by reducing the degradation rate of BPQDs. It should also be noted that NMP is an organic solvent that may raise toxicity concerns. Therefore, we suggest that oxygen-free water may be used to exfoliate bulk BP and prepare phosphorene materials in future studies. Through this method, both concerns regarding toxicity and oxidation can be avoided. In addition, to increase the concentration of Xene-based therapeutics at disease sites for improved therapeutic efficacy, targeting linker functionalization of the Xenes is one of the most commonly used strategies. For instance, Tao *et al.* reported a folic acid (FA)-functionalized phosphorene delivery platform for effective targeted delivery of chemotherapeutic drug doxorubicin (DOX) to tumour sites in a human cervical

cancer HeLa xenograft tumour model.[10] Also, Zeng and co-workers developed a single-stranded oligonucleotide aptamer (Apt)-functionalized phosphorene delivery platform for effective target co-delivery of DOX and siRNA to tumour sites in human breast cancer MCF-7 xenografts.[40] Both targeted delivery platforms showed significantly enhanced tumour accumulation and improved therapeutic efficacy compared to their corresponding non-targeted modalities.

4.2 Biosensors

Because of their extremely low concentrations in clinical blood samples, detection of targeted biomarkers usually requires the development of highly specific and sensitive biosensors in biomedical fields. In this section, Xene-based biosensors (*e.g.*, field effect transistor biosensors, electrochemical biosensors, fluorescent biosensors, colorimetric biosensors, and gas sensors) are discussed.

2D Xenes possess unique electrical and physical characteristics, and are ideal candidates for fabrication of biosensors for the detection of biomolecules such as glucose, hormones, proteins, enzymes, and DNA strands. Silicene (2D Si) and germanene (2D Ge) play important roles as conducting channels in FET biosensors, due to their excellent electron transport properties in contact with metal conductors. They are generally devised to transform biomacromolecules' binding information at the solid/liquid interface into detectable electronic outputs with high selectivity and sensitivity (Fig. 9a).[41] In addition, a silicene based DNA electrochemical biosensor was also developed, allowing specific recognition of the single stranded DNA counterpart, as an integrated-circuit biosensor for the fabrication of a lab-on-a-chip device for DNA sequencing.[42]

Group VA elements, also called pnictogens, such arsenene (2D As), antimonene (2D Sb), and bismuthene (2D Bi), might offer better stability to enhance the biosensing performance stemming from their intrinsic heavier weight. Therefore, these 2D layered pnictogen thin nanosheets prepared by shear-force exfoliation methods were fabricated as electrochemical biosensors using a layer-by-layer approach, which significantly enhanced their analytical performance in terms of selectivity and sensitivity for the detection of chemical substances, such as phenol.[43] Due to its low oxidation-to-bulk ratio and prominent electrocatalytic property, antimonene showed a high efficiency for the detection of phenol. The phenol limit of quantitation (LOQ; ~850 nm) and limit of detection (LOD; ~250 nm) were improved ~10 times compared to recommended analytical accuracy. In another study, an antimonene-based surface plasmon resonance (SPR) sensor with a LOD of ~10 aM was developed in order to detect microRNA (miRNA), an important biomarker for cancer diagnosis. Briefly, single stranded DNA (ssDNA) decorated antimonene nanosheets were successfully prepared to pair up the complementary miRNA analyte. Correspondingly, the amount of miRNA was recognized by a change in the SPR angle (Fig. 9b). Furthermore, the present antimonene material based clinically relevant SPR point-of-care (POC) platform enabled a large enhancement of the detection efficiency compared to conventional miRNA quantification techniques, such as q-PCR and northern blotting.[12]

Phosphorene has also aroused great interest in biosensor fabrication recently (Fig. 9c). In FET devices, phosphorene has

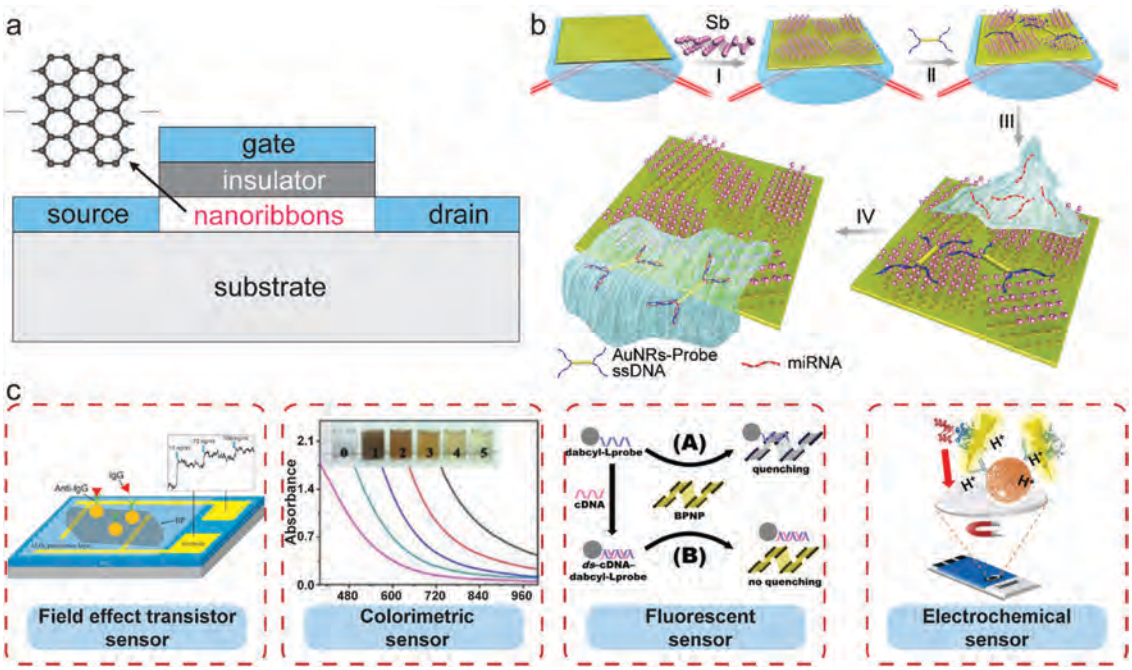

Fig. 9 Emerging Xene-based biosensors. (a) Schematic of a field effect transistor device fabricated using silicene. Reprinted with permission from ref. 41. Copyright 2014 IOP Publishing Ltd. (b) Fabrication of a miRNA sensor integrated with antimonene nanomaterials. Reprinted with permission from ref. 12, Copyright 2019 Nature Publishing Group. (c) Phosphorene has been widely used in biosensing, as field effect transistor sensors, colorimetric sensors, fluorescent sensors and electrochemical sensors. Reprinted with permission from ref. 37, Copyright 2018 Ivyspring International Publisher.

demonstrated higher hole mobility with reduced current fluctuation. Gold nanoparticle-decorated phosphorene showed excellent 4-nitrophenol (4-NP)-reduction catalytic activity, providing a colorimetric signal output from yellow 4-NP to colorless 4-aminophenol (4-AP), which is adapted to detect the carcinoembryonic antigen biomarker as a highly selective and sensitive colorimetric method in the clinical samples obtained from breast and colon cancer patients.[37] Moreover, a phosphorene nanosheet fabricated biosensor was developed for detection of H_2O_2, an essential mediator in biomedicine, *via* a supercritical carbon dioxide (CO_2)-assisted rapid synthesis. It exhibited an efficiency enhancement of $\sim$20 times compared to regular electrochemical methods. Phosphorene nanosheets were also developed as clinical diagnostic platforms for label-free detection of myoglobin (*i.e.*, a significant cardiovascular disease biomarker) *via* a co-functionalization of negatively charged nucleic acid aptamers and cationic polymer poly-L-lysine (PLL).[37] In addition, downsizing of layered phosphorene microparticles to nanoparticles was accompanied by enhanced electrocatalytic activity *via* a hydrogen evolution mediation. Coupled with linear sweep voltammetry and electrochemical impedance spectroscopy, phosphorene provided a new vision in biosensing technology for rabbit immunoglobulin G (IgG) detection with an LOD of less than 1 ng mL^{-1}.[37] However, phosphorene is unstable in air, and its instability leads to other layered monoelements despite its small band gap and high carrier mobility. To overcome these limitations, band gap engineering combining the advantages of two or more monoelements through heterostructures is proposed. For example, sandwiched heterostructures obtained by encapsulating atomically thin black phosphorus with boron nitride layers remain ultra-stable interfaces under ambient conditions, demonstrating their high-speed electronic and optoelectronic performances in biomedical sensing.[44]

4.3 Bioimaging

Noninvasive bioimaging is valuable for a diagnostic process which could reduce unnecessary biopsies and facilitate therapy subsequently. Bioimaging based on Xenes has been reported to show superior performance to other traditional imaging technologies, which facilitate diagnosis-guided therapeutic strategy. Xene-based bioimaging applications (PAI, PTI, FI, CT, and PLTI) are discussed in this section.

PAI is an emerging diagnostic modality, which can break through the penetration limits of purely optical imaging modalities by the detection of laser-irradiated tissue-induced pressure waves. Due to its low tissue-attenuation coefficient, the detection of functional information and biological structures can thus be achieved in a real-time manner. Other advantages also include depth-resolved 3D imaging, spatial resolution, and high sensitivity. A good photothermal conversion ability is a necessity for an efficient PAI contrast agent and can guarantee significant PA signal levels in contrast to the surrounding tissues. Xenes are among the most attractive PAI agents because of their superior photothermal conversion. For example, borophene (2D B) nanosheets were demonstrated with excellent PA properties, which originated from their high NIR-light-to-heat conversion efficiency ($>$40%), and used successfully for *in vivo* PAI in a breast cancer xenograft mouse model (Fig. 10a).[14] Other forms of Xenes have also been reported for *in vivo* PAI, such as antimonene (2D Sb) nanosheets,[6] tellurene (2D Te) nanosheets,[11] ultrasmall bismuth (2D Bi) nanoparticles,[45] and phosphorene (2D BP) nanoparticles.[46]

Non-fluorescent objects can hardly be detected optically if the optical wavelength is considerably bigger than their size, and scattering cross sections are small. But if they can absorb the light and then convert it into heat, then detection can be enabled in another form (*i.e.*, PTI). PTI can also be used to monitor the temperature changes during the *in vitro* and *in vivo* applications of Xene-based photothermal agents (*e.g.*, assessment of the *in vitro* photothermal conversion and the *in vivo* PTT effect). In general, all these photothermal agents designed for PTT need to be verified by PTI. For example, novel antimonene (2D Sb) nanosheet[6] (Fig. 10b) and QD[7] based photothermal agents with ideal photothermal conversion efficacy and biocompatibility were developed using different controllable liquid exfoliation methods, leading to superior NIR photothermal performances as verified by PTI. PAI and PTI techniques, combining the high contrast of light with a large penetration depth capacity of ultrasound, are usually conjunctively used and have been demonstrated with great potential for bioimaging.[6,14,45]

FI, which enables various levels of experimental observations, is the visualization of molecular processes or structures in cells and tissues using fluorescent dyes as labels. Xenes can be used to effectively load these fluorescent dyes for FI because of their ultrahigh surface area-to-volume ratios, which can enable a high capacity of dye attachment. For example, a dye-labeled, phosphorene (2D BP) nanosheet-based delivery platform is developed for both intracellular mechanistic understanding (*e.g.*, intracellular trafficking pathways) of 2D nanomaterials and *in vivo* biodistribution analysis (Fig. 10c).[10] Fluorescein isothiocyanate (FITC)-labeled PEGylated phosphorene nanosheets are reported to enter HeLa cells *via* the "caveolae-dependent endocytosis $\rightarrow$ early endosomes $\rightarrow$ late endosomes" and "macropinocytosis $\rightarrow$ late endosomes $\rightarrow$ lysosomes" pathways. Such a study can provide deep insights into the intracellular fate of developed nanomaterials.[47] In another report, Cy7-attached PEGylated phosphorene nanosheets are used for *in vivo* imaging and demonstrated a high accumulation in a cervical cancer xenograft mouse model, which is promising for *in vivo* therapeutic studies. Antimonene (2D Sb) nanosheets and borophene (2D B) nanosheets have also been reported for *in vitro* and *in vivo* FI.[6,14]

CT, also called X-ray-computed tomography, is one of the most popular bioimaging techniques, which utilizes ionizing radiation for imaging by means of special computer-aided X-ray equipment. CT is able to produce 3D images of biological tissues and fine cross-sections with high resolution and deep penetration. Besides its application in scanning soft tissues (*e.g.*, cardiovascular tissue and coronary arteries), CT is also preferred for noninvasive tumour detection and painless verification of location, size, and shape. Xene-based nanomaterials also have great potential in the application of CT imaging. For example, bismuth, whose K-edge value (90.5 keV) and X-ray attenuation parameters are much larger than those of a clinical iodine-based contrast agent (33.2 keV), possesses great potential for CT imaging.

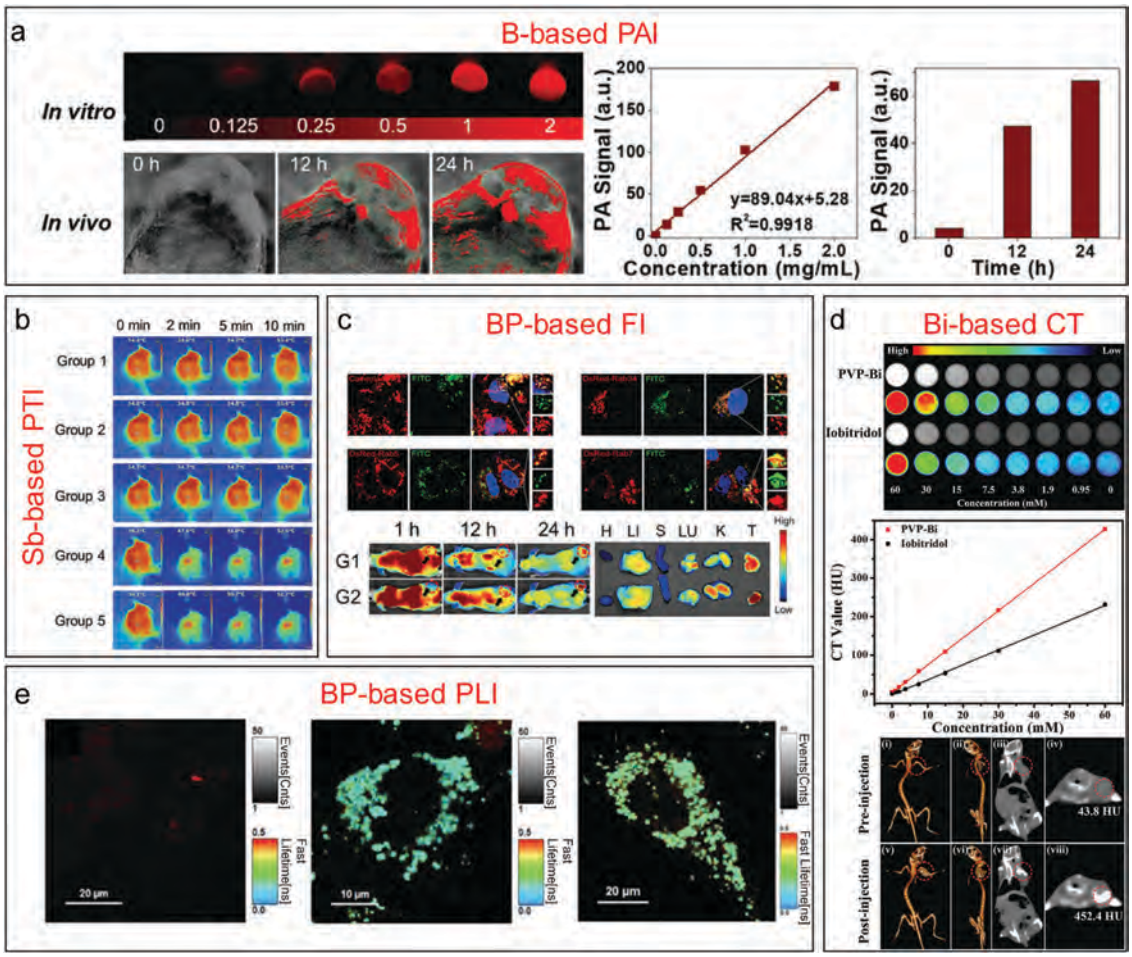

Fig. 10 Emerging Xene-based bioimaging. (a) Borophene-based photoacoustic imaging (PAI). Reprinted with permission from ref. 14, Copyright 2018 Wiley. (b) Antimonene-based photothermal imaging (PTI). Reprinted with permission from ref. 6, Copyright 2018 Wiley. (c) Phosphorene-based fluorescence imaging (FI). Reprinted with permission from ref. 10, Copyright 2017 Wiley. (d) Bismuthene-based X-ray computed tomography (CT) imaging. Reprinted with permission from ref. 8, Copyright 2017 Wiley. (e) Phosphorene-based photoluminescence lifetime imaging (PLTI). Reprinted with permission from ref. 9, Copyright 2018 American Chemical Society.

In a report by Lei *et al.*, PVP-coated ultrasmall bismuth (2D Bi) nanodots showed an ~3 times CT contrast resolution enhancement compared to those of conventional iodine agents in the clinic (Fig. 10d).[8] In another report by Yu *et al.*, cyclic peptide (CGNKRTRGC, LyP-1) modified ultrasmall bismuth (2D Bi) nanoparticles were developed and demonstrated with a significantly higher slope of Hounsfield units (13.8 HU mM^{-1}, HU value) than iohexol (4.28 HU mM^{-1}).[45] In addition, as a recognized "green metal" that is inexpensive and nontoxic, bismuthene has unique advantages in potential clinical CT imaging.

Despite its simplicity and accuracy in laboratory standards, FI may be inadequate in real-world situations. The probe/agent concentration at each point of the image can hardly be detected, and the changes in fluorescence intensity may be caused by photo-transformation, photobleaching, and/or diffusive processes. However, PLTI can provide complementary and/or unique information from the fluorescence lifetime of fluorophores. In addition, with advantages such as high sensitivity to a real-time microenvironment, PLTI is widely used to dynamically detect the influence of environmental factors on pathophysiological progress and the micro-environment in living cells. For example, Meng *et al.* developed novel phosphorene (2D BP) nanoparticles with an average lateral size of ~35 nm and used them as an efficient agent for live cell imaging (Fig. 10e).[9] The fabricated phosphorene nanoparticles had a photoluminescence lifetime (PLT) of 110.5 ps and a photoluminescence emission at a wavelength of ~690 nm. The PLT of the phosphorene nanoparticles is demonstrated to be sensitive to ionic strength and the intracellular microenvironment, indicating promising applications as probes for sensing variations of the cellular microenvironment and cells with distinct cytosolic contents. Lee *et al.* also demonstrated phosphorene (2D BP) nanodots (an average diameter: ~10 nm) as a biological fluorescent agent.[48]

4.4 Therapeutic applications

A number of emerging Xenes have been well-developed for different therapeutic applications. Due to their excellent electronic and optical properties, Xenes usually have a broad absorption spectrum across the UV, visible-light and NIR regions, as well as the ability to effectively generate local hyperpyrexia or cytotoxic

reactive oxygen species (ROS) upon irradiation. Thus, the emerging Xenes can be employed in cancer phototherapies such as PTT and PDT, which offer unique advantages including minimal invasiveness and effective therapeutic efficacy. In addition, Xenes have also been utilized as drug delivery systems for disease treatment because of their ultra-high specific surface area with high drug-loading capacity and NIR light and/or moderately acidic pH-triggered drug-release.

As a robust technique for cancer therapy, PTT can generate local hyperpyrexia under NIR laser irradiation to effectively kill cancer cells. Compared with traditional therapeutic methods such as chemotherapy and surgery, the therapeutic effect of PTT only occurs at disease sites with both NIR laser exposure and photothermal agent accumulation, generating unique advantages such as high selectivity, ease of the procedure, minimal invasiveness, and low/no systemic toxicity. The precondition for effective PTT is developing satisfactory photothermal agents with good biocompatibility and high photothermal conversion efficiency. The emerging Xenes, which (1) exhibit strong/broad absorption from the UV to NIR range (optical and electronic properties) and (2) possess simple and nontoxic monoelements (chemical properties), provide exciting opportunities for the development of promising photothermal agents. For example, we, for the first time, developed antimonene (2D Sb) QDs and verified their great potential in PTT.[7] The antimonene QDs, named AMQDs in the published report, were prepared *via* a combined liquid-phase exfoliation method in ethanol (Fig. 11a). After PEGylation, the synthesized PEG-coated antimonene QDs showed excellent biocompatibility and good stability in the physiological medium. The obtained antimonene QDs exhibited broad and strong light absorption from the UV range to the NIR region, indicating that they may exhibit remarkable photothermal properties. As expected, when the concentration of antimonene QDs was 200 μg mL^{-1}, the temperature increased by 50 °C within 5 min under NIR laser irradiation (808 nm, 2 W cm^{-2}). Besides, the photothermal conversion efficacy of PEG-coated antimonene QDs was calculated to be 45.5%, which is higher than those of a variety of previously reported photothermal agents. Furthermore, the *in vitro* experimental results confirmed that the PEG-coated AMQDs showed good biocompatibility without any significant cytotoxicity to a variety of cell lines including A549 (human lung carcinoma cells), HeLa, PC3 (human prostate cancer cells), MCF-7, and HEK 293 (normal human embryonic kidney cells), while the tumour cells were almost completely eliminated by PTT. The *in vivo* results demonstrated that the PEG-coated AMQDs had excellent photothermal effects in an MCF-7 xenograft model (intratumoral injection) without recurrence and any noticeable side effects (Fig. 11b). Considering the fact that antimonial drugs have been applied in medicine for a long history, these findings further confirmed that the PEG-coated antimonene QDs have great potential for use as a biocompatible photothermal nanoagent. Besides the antimonene QDs, other forms of Xenes recently reported as photothermal agents for PTT include phosphorene (2D BP) QDs,[36] phosphorene (2D BP) nanosheets,[49] phosphorene (2D BP) nanoparticles,[46] ultrasmall bismuth (2D Bi) nanoparticles,[45] ultrasmall bismuth (2D Bi) nanodots,[8] and tellurium nanodots (2D Te).[50] As another form of phototherapy, PDT elicits cell death (phototoxicity) by radicals and/or ROS generated from a photosensitizing chemical substance (*i.e.*, photosensitizer) under light irradiation. The light source needs to possess the appropriate wavelength for exciting the photosensitizer. PDT has been clinically approved to treat a variety of diseases (*e.g.*, malignant cancers, atherosclerosis, psoriasis, *etc.*) and widely recognized as a therapeutic strategy with minimal invasiveness and minimal toxicity. Other advantages also include no need for delicate surgery and/or lengthy recuperation, and no formation of disfigurement and/or scar tissue. Similar to PTT, PDT only generates therapeutic effects in target disease sites with photosensitizer accumulation and light irradiation, while not damaging the neighboring healthy tissue. The emerging Xene-based photosensitizers provide new opportunities for overcoming the current limitations (*e.g.*, narrow light absorption, easy photobleaching, low quantum yields, poor biocompatibility) of traditional PDT strategies in biomedical applications. For example, Wang *et al.* first demonstrated that ultrathin phosphorene (2D BP) nanosheets have the capability to generate singlet oxygen ($^1O_2$) with a high quantum yield of 0.91 under 660 nm light irradiation. Both *in vitro* and *in vivo* experimental results demonstrated that the phosphorene nanosheets show a noteworthy PDT capability, photodegradation properties, and good biocompatibility, which means that the BP nanosheets have great potential for use as a photosensitizer.[51] In another report, Lin *et al.* developed free-standing tellurene (2D Te) nanosheets through a liquid-phase exfoliation method in DMF and engineered the obtained nanosheets as promising PDT agents (Fig. 11c).[11] Under 670 nm light irradiation, the prepared nanosheets effectively produced $^1O_2$ (Fig. 11d), resulting in potent intracellular ROS enhancement to kill tumour cells (Fig. 11e). The *in vivo* PDT therapeutic effect of the engineered tellurene nanosheets was further verified in HepG2 liver tumour-bearing nude mice. As shown in Fig. 11f, significant *in vivo* therapeutic effects only occurred in the group that was co-treated with both the developed nanosheets (*via* intratumoral injection) and light illumination. The hematoxylin and eosin (H&E) staining images further demonstrated that the co-treatment of nanosheets and light can lead to serious destruction of tumour sites compared to control groups, indicating the promising application of these tellurene nanosheets in PDT. The other reported forms of Xenes that have been applied to PDT successfully include phosphorene (2D BP) QDs[52] and tellurium (2D Te) nanodots.[50]

Drug delivery systems are engineered platforms to overcome different physiological barriers for effective/targeted delivery of various drugs (*e.g.*, small molecule drugs, RNAs, DNAs, peptides, and proteins) and on-demand release of therapeutics. With tremendous efforts contributed by biomedical engineers and several delivery platforms that have been introduced into clinical practices, the substantial development of drug delivery strategies is expected to revolutionarily change the landscape of the biotechnology and pharmaceutical industries in the near future. Due to their unique morphologies (*e.g.*, ultrahigh surface area-to-volume ratios and ultrathin 2D structures), tunable compositions (*e.g.*, selection of different monoelements), and functional nanostructures, the emerging Xene-based delivery platforms have been

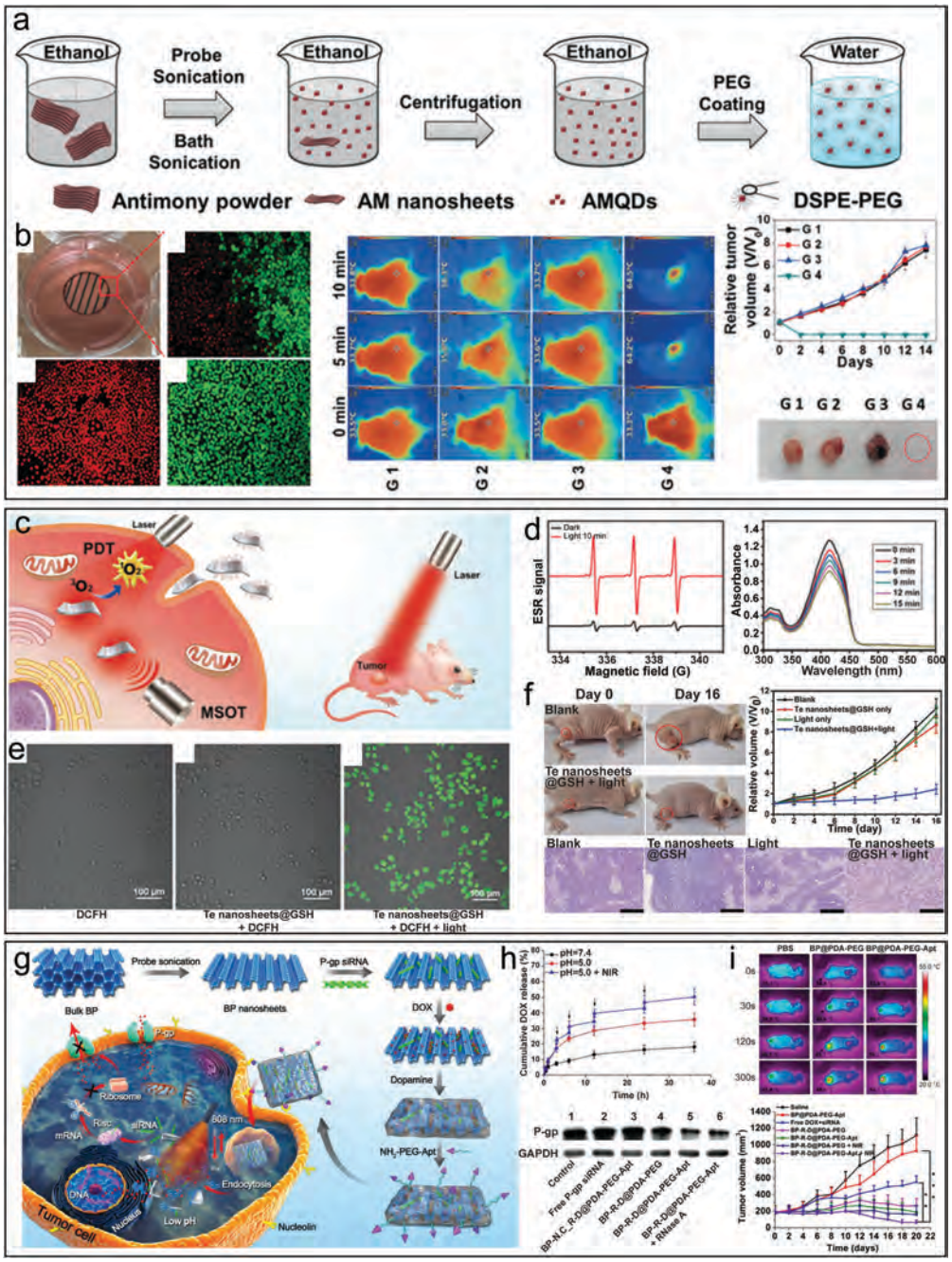

Fig. 11 Emerging Xene-based therapeutic applications. (a and b) Antimonene-based photothermal therapy (PTT). Reprinted with permission from ref. 7, Copyright 2017 Wiley. (c–f) Tellurene-based photodynamic therapy (PDT). Reprinted with permission from ref. 11, Copyright 2018 Royal Society of Chemistry. (g–i) Phosphorene-based drug delivery systems. Reprinted with permission from ref. 40, Copyright 2018 Wiley.

investigated. For example, our group for the first time reported the engineering of phosphorene (2D BP) nanosheets for the delivery of DOX.[10] The phosphorene nanosheets were coated with PEG-NH_2 to obtain PEGylated phosphorene nanosheets. The prepared nanosheets possessed a high drug-loading capacity of ~108%, which is much higher than the reported nanoparticle-based material system (usually 10–30%). It is noteworthy that the NIR photothermal effect of these nanosheets could control/accelerate the drug release from the delivery platform. Both *in vitro* and *in vivo* results verified that PEGylated phosphorene nanosheets are promising as a robust drug delivery platform with good biocompatibility. Soon afterward, Chen *et al.* also applied phosphorene nanosheets as a platform for DOX delivery and showed an ultrahigh DOX loading capacity (950%) and a significant PTT/PDT/chemotherapy synergistic anti-tumor effect.[49] Compared with the first phosphorene-based delivery platform reported by our group,[10] the much higher DOX loading capacity may be caused by the following two factors: (i) without the shielding of the PEGs, all the surface area can be used for DOX loading and (ii) larger nanosheet size could lead to larger

surface area for more attachments. Followed by this representative paradigm, more and more phosphorene-based[26,40] and other forms of Xene-based delivery platforms (*e.g.*, 2D Sb and 2D B)[6,14] have been developed very recently. For example, Zeng *et al.* reported a modified phosphorene-based platform for co-delivery of P-gp siRNA and DOX against multidrug-resistant breast cancer models (Fig. 11g).[40] Polydopamine (PDA)-coating endowed this co-delivery platform a higher photothermal conversion efficiency and better stability compared to a bare phosphorene-based platform. In addition, pH and NIR irradiation stimulated the release of both chemotherapeutic drugs (DOX) and gene therapeutic agents (P-gp siRNA) (Fig. 11h). The *in vivo* experimental results exhibited a prominent synergistic therapeutic effect against multidrug-resistant breast cancer (Fig. 11i). Similarly, to stabilize phosphorene (*i.e.*, inhibiting the rapid degradation of phosphorene), BP/Bi_2O_3 heterostructures were prepared as stable and efficient sensitizers for synergistic cancer radiotherapy with good biocompatibility.[53] Although the results in these studies are very encouraging and promising, therapeutic exploration of Xenes is still relatively new compared to that of other 2D materials. Many critical issues including stability, degradation, biosafety and biocompatibility still need to be systematically investigated before pervasive therapeutic applications.

4.5 Theranostics

By integrating both therapeutic and diagnostic functions, theranostics represent an emerging modality of nanomedicine, which enables simultaneous diagnosis, therapy, and real-time monitoring of treatment response. An early recognition/diagnosis of specific diseases can be achieved using theranostic agents through personalized therapy guided by different imaging modalities. The whole journey of the theranostic agents in biosystems or the human body (*e.g.*, distribution, absorption, metabolism, and excretion) can be closely detected *via* different imaging techniques, which can contribute to better therapeutic outcomes and minimal side effects. The emerging Xenes provide a library of theranostic agents because of their intrinsic properties for both effective therapy (*e.g.*, PTT, PDT, and radiotherapy) and multimodal imaging (*e.g.*, PAI, PTI, FI, CT, and PLTI). In addition, cargo loading and/or surface modification can be easily achieved through simple synthetic steps for the reinforcement and diversification of the current library of Xenes. For instance, diverse drugs and/or fluorophores can be loaded onto the surfaces of Xenes to generate new theranostic functions (*e.g.*, small molecule drugs for combined chemotherapy, RNAs/DNAs for gene therapy, *etc.*).

In 2017, a novel theranostic agent based on ultrasmall bismuth (2D Bi) nanoparticles (~3.6 nm) was facilely developed with oleylamine as a reducing agent for cancer therapy (Fig. 12a and b).[45] Through the surface modification of tumour-homing peptide LyP-1 and PEGylation with DSPE-PEG_{5000}, the prepared Bi-based nanoparticles showed a higher tumour accumulation. Their excellent abilities to absorb both second near-infrared (NIR-II) window laser radiation and ionizing radiation enabled the developed Bi-based nanoparticles to be promising agents for dual-modal PAI/CT imaging (Fig. 12c and d). In addition, a synergistic treatment by the combination of PTT and radiotherapy can also be efficiently achieved (Fig. 12e and f). In addition, rapid and complete clearance of nanoparticles with low toxicity was also demonstrated. Meanwhile, Lei *et al.* also synthesized ultrasmall PVP-protected bismuth (2D Bi) nanodots,[8] which could achieve X-ray CT/PAI dual-modal imaging-guided PTT for precise tumor treatment, indicating the great potential of PVP@Bi nanodots as safe and powerful Xene-based nanotheranostic agents. As mentioned in the above section, antimonene (2D Sb) has a high photothermal conversion efficiency and an excellent photothermal effect, and its ultrathin 2D structure makes it worth expecting as a drug delivery platform. In 2018, our group synthesized antimonene nanosheets (named AM NSs in the published report) through a liquid-phase exfoliation and employed them to load chemotherapeutic drugs (*e.g.*, DOX) and FI agents (*e.g.*, Cy5.5) as multimodal-imaging-guided cancer theranostics (Fig. 12g).[6] The obtained PEGylated antimonene nanosheets with an average size of ~90 nm exhibited a superior photothermal conversion efficiency (41.8%) and a high drug loading capacity (150.0%). Meanwhile, triggered/controlled release of the therapeutic was easily realised by exposure to moderately acidic pH and NIR radiation. More importantly, the reported antimonene-based nanomedicine showed preferable tumour accumulation (Fig. 12h) and *in vivo* deep tumour penetration of the cargo under the NIR laser irradiation (Fig. 12i). With the imaging guidance of FI/PAI/PTI, the DOX-loaded PEGylated antimonene nanosheets showed prominent tumour growth inhibition *in vivo* (Fig. 12j). No observable side effects were reported during the treatment period. As the first report on antimonene-based drug delivery platforms, we expect a jumping-off point (inspired by this study) for the theranostic application of antimonene. Other forms of Xenes have also been reported in this category that includes borophene (2D B) nanosheets,[14] phosphorene (2D BP) nanosheets,[10] and ultrasmall bismuth (2D Bi) nanodots.[8] Although preliminarily theoretical and experimental studies have been performed to support the potential of Xene materials, their investigations still focus on the material synthesis, characterization, and preliminary theranostic evaluation. Further and more in-depth exploitations of Xene expertise regarding nano–bio interactions, metabolism, and toxicity are highly desired for clinical transformation.

4.6 Other biomedical applications

Exploring new scenarios in biomedical applications has always been a research focus for Xenes. Besides the above-discussed applications, other new modalities of biomedical applications such as antimicrobials, neuroprotective nanomedicine, and bone regeneration have been reported very recently. Current pioneering studies are majorly focused on phosphorene for the following reasons like (1) phosphorene (2D BP) is well-recognized as the next representative after graphene for a relatively longer time than other emerging Xenes, and (2) most of the other emerging Xenes are in the theoretical stage or just experimentally prepared very recently. Taking phosphorene as an example, this section explores several areas of opportunity where the emerging Xenes may enable entirely novel classes of biomedical applications.

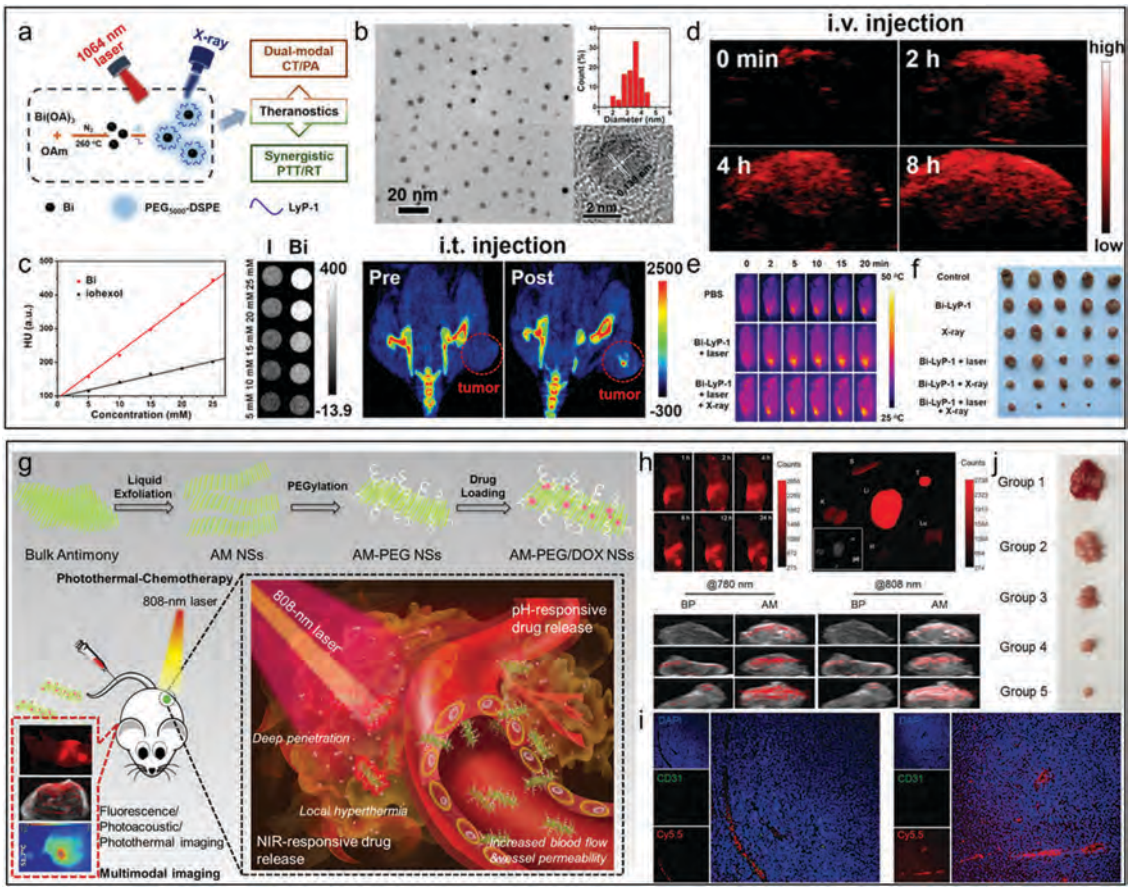

Fig. 12 Emerging Xene-based theranostics. (a–f) Bismuthene-based dual-modal CT/PAI-guided synergistic PTT/radiotherapy. Reprinted with permission from ref. 45, Copyright 2017 American Chemical Society. (g–j) Antimonene-based FI/PAI/PTI guided synergistic chemo-photothermal therapy. Reprinted with permission from ref. 6, Copyright 2018 Wiley.

Ouyang *et al.* presented an efficient, convenient and general approach to decorate Ag nanoparticles on the surfaces of phosphorene nanosheets through an *in situ* growth strategy (named Ag@BP in this report) (Fig. 13a).[54] In these Ag@BP nanohybrids, phosphorene nanosheets played a triple role (*i.e.*, acting as a supporting substrate, a reductant, and a stabilizer) for the formation and stabilization of Ag nanoparticles (Fig. 13b). More importantly, the phosphorene nanosheets and Ag nanoparticles combined together in the Ag@BP nanohybrids, leading to a synergistic antibacterial effect. The Ag nanoparticles on the phosphorene nanosheets did not affect the photothermal effect of the developed Ag@BP nanohybrids and the resulting material possessed high photostability. Moreover, the excellent photothermal effect of the Ag@BP nanohybrids can also accelerate the release of silver ions from Ag nanoparticles. The *in vitro* results demonstrated that most of the bacteria were eliminated within a minutes *via* the photothermal effect coming from the phosphorene nanosheets under NIR laser irradiation. Subsequently, the Ag nanoparticles in the Ag@BP nanohybrids accelerated the sustainable release of Ag^{+} due to the photothermal effect and further inhibited methicillin-resistant *Staphylococcus aureus* (MRSA) proliferation (Fig. 13c). The most attractive point in this investigation was that the antibacterial mechanism of the Ag@BP nanohybrids was mainly mediated through local hyperthermia and oxidative stress, which overcame the problem of antibiotic resistance. Furthermore, the *in vivo* studies demonstrated that the Ag@BP nanohybrids with excellent biocompatibility exhibited significant synergistic performance in eliminating MRSA bacteria and alleviating skin infection.

In another report, Chen *et al.* reported that Cu^{2+} could be efficiently captured by phosphorene nanosheets, thus protecting neuronal cells from Cu^{2+}-induced neurotoxicity (Fig. 13d).[55] The phosphorene nanosheets showed a superior Cu^{2+} capture capacity of 0.86 mmol g^{-1} and a high selectivity toward Cu^{2+}. Furthermore, the phosphorene nanosheets could inhibit Cu^{2+}-catalyzed production of ROS. It is well known that Cu^{2+} can oxidize ascorbic acid (AA) to produce H_2O_2. In preliminary experiments, in the absence of phosphorene nanosheets, almost all of AA was oxidized by Cu^{2+} and about 27 μm of H_2O_2 was produced within 1 h. However, AA could hardly be oxidized by Cu^{2+} and no H_2O_2 was generated in the presence of phosphorene nanosheets. The *in vitro* studies demonstrated that the phosphorene nanosheets inhibited the production of intracellular ROS induced by Cu^{2+} and protected SH-SY5Y cells (human neuroblastoma cell line) from ROS damage. More importantly, the permeability of the phosphorene nanosheets across the blood–brain barrier (BBB)

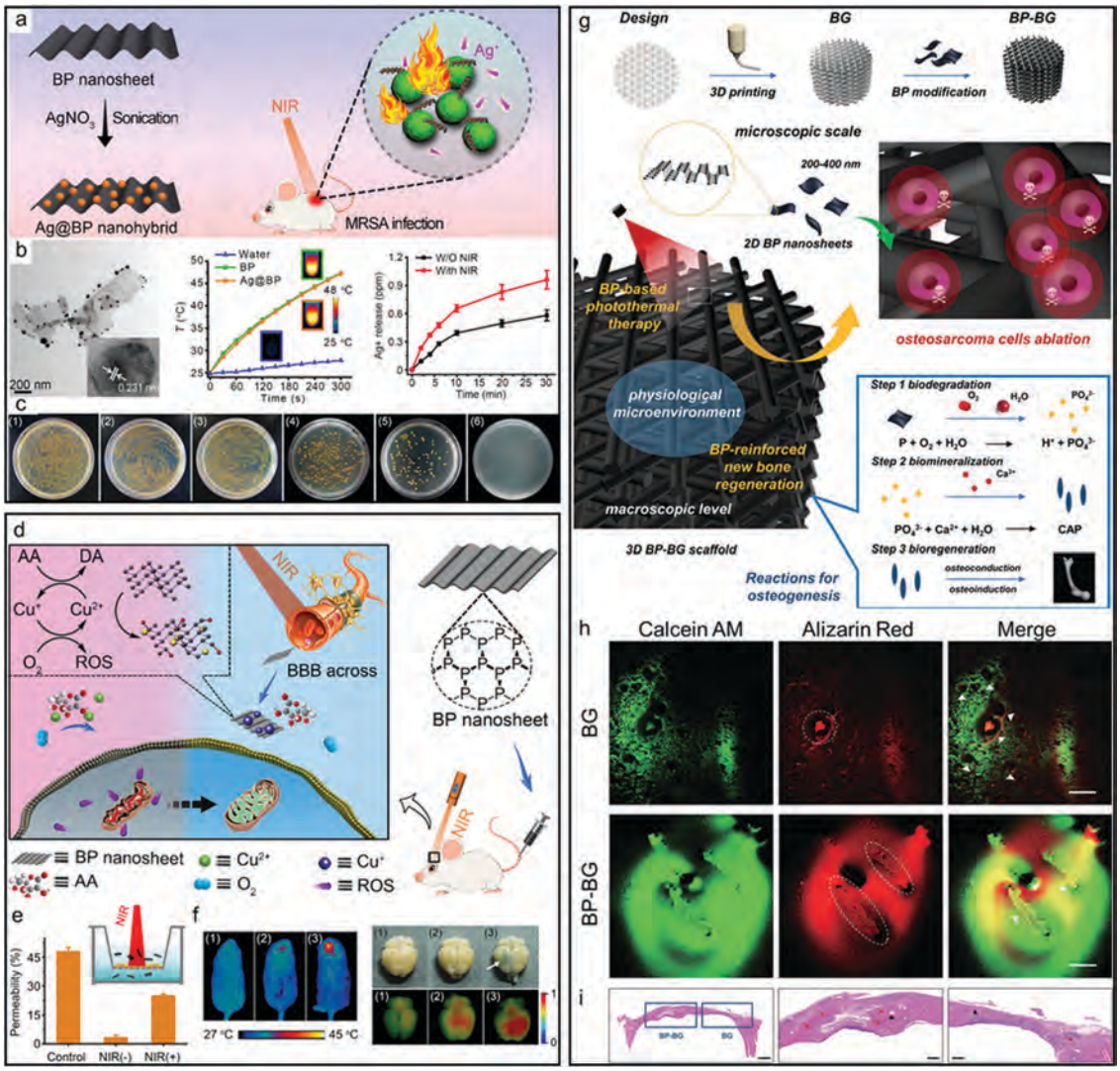

Fig. 13 Emerging Xene-based other new modalities of biomedical applications. (a–c) Phosphorene-based antimicrobial application. Reprinted with permission from ref. 54, Copyright 2018 Royal Society of Chemistry. (d–f) Phosphorene-based neuroprotective nanomedicine for neurodegenerative disorder therapy. Reprinted with permission from ref. 55, Copyright 2018 Wiley. (g–i) Phosphorene-based application in bone regeneration. Reprinted with permission from ref. 56, Copyright 2018 Wiley.

increased significantly due to the excellent photothermal effect of the phosphorene nanosheets. An *in vitro* BBB model experiment showed that the amount of phosphorene nanosheets that crossed the BBB simulation barrier and transported to a lower chamber was increased from 3.5% to 48% after NIR laser irradiation (Fig. 13e). The *in vivo* results showed that Evans blue dye could cross the BBB and stain the brain due to the photothermal effect of the phosphorene nanosheets. The brains of mice treated with Cy5-labeled PEGylated phosphorene nanosheets and NIR irradiation exhibited the strongest NIR fluorescence intensity (Fig. 13f). These results confirmed that the photothermal effect could enhance the BBB permeability of the phosphorene nanosheets. Therefore, phosphorene nanosheets with good biocompatibility and stability are promising to serve as a neuroprotective agent for neurodegenerative disorder therapy.

Very recently, phosphorene has also been reported to have great potential in the application of bone regeneration. Yang *et al.* designed a novel and exquisite therapeutic platform based on a phosphorene reinforced 3D-printed scaffold, which can improve bone regeneration after localized osteosarcoma therapy through photothermal ablation (Fig. 13g).[56] Notably, the intrinsic physiochemical properties of phosphorene nanosheets which can easily undergo oxidation to form PO_4^{3-} enable them to exhibit outstanding performance for *in situ* biomineralization due to the strong coordination between PO_4^{3-} and calcium ions in the physiological environment (Fig. 13h and i). These multifunctional 3D-printed scaffolds that can achieve *in situ* phosphorus-driven biomineralization may provide a better understanding on the mechanisms of osteogenesis and motivate further developments in Xene-guided bone-tissue engineering.

In summary, we expect that an increasing number of new modalities of biomedical applications will be inspired by these pioneering studies. Table 1 lists the biomedical applications of Xenes, such as biosensors, bioimaging, therapeutic applications,

Table 1 Emerging Xenes for different biomedical applications and the corresponding periodic table groups, synthesis methods, and modification strategies

Periodic table group	Element	2D form	Synthesis methods	Morphology	Biomedical application	Surface modification	Ref.
III	B	Borophene	PVD, mechanical cleavage, etching, and liquid-phase exfoliation	Nanosheets	PTT, PAI, drug delivery, FI	PEG_{2000}-NH_2	4 and 14
III	Ga	Gallenene	PVD and solid–melt exfoliation	Nanosheets	N.A.	N.A.	18 and 19
IV	Si	Silicene	PVD and chemical exfoliation	Nanosheets	Biosensors	Alkali metal	21 and 22
IV	Ge	Germanene	Mechanical cleavage and PVD	Nanosheets	N.A.	N.A.	2, 15 and 23
IV	Sn	Stanene	PVD	Nanosheets	N.A.	N.A.	24
V	P	Phosphorene	Mechanical cleavage, liquid-phase exfoliation, etching, CVD, PVD, and wet-chemistry	Nanosheets, nanoparticles, and quantum dots	Biosensors, PAI, PTI, drug delivery, PTT, PDT, FI, PLTI, antimicrobials, neuroprotective nanomedicine, bone regeneration, *etc.*	PEG_{2000}-NH_2, PLGA, agarose gel, Ag nanoparticles, Cu^{2+}, polydopamine, *etc.*	5, 9, 10, 15, 26, 40, 49, 51 and 54
V	As	Arsenene	Mechanical cleavage and liquid-phase exfoliation	Nanosheets	Biosensors	N.A.	13, 27 and 43
V	Sb	Antimonene	Mechanical cleavage, PVD, and liquid-phase exfoliation	Nanosheets and quantum dots	Biosensors, PAI, PTI, FI, drug delivery, PTT	DSPE-PEG_{3000}, ssDNAs	6, 7, 13 and 28
V	Bi	Bismuthene	Mechanical cleavage, PVD, and liquid-phase exfoliation	Nanodots, nanosheets, and nanoparticles	PAI, PTI, PTT, CT, RT, biosensors	PVP, DSPE-PEG_{5000}, LyP-1 peptide	2, 13, 15, 31 and 43
VI	Se	Selenene	PVD	Nanosheets	N.A.	N.A.	33
VI	Te	Tellurene	Wet-chemistry, liquid-phase exfoliation, and PVD	Nanosheets and nanodots	PTT, PDT, PAI, PTI	HSA, GSH, PVP	11, 34, 35 and 50

theranostics, and other new forms of applications (*e.g.*, antimicrobials, neuroprotective nanomedicine, and bone regeneration).

5. Conclusions and perspectives

This review systematically classifies and summarizes the recent developments of the emerging Xenes in terms of their synthesis methods, inherent properties and various biomedical applications (Table 1). We also provide our critical insights in the following discussions, aiming at placing the emerging Xenes in the pole position for innovative bio-nanotechnologies.

Although many research studies demonstrate the great potential of Xenes in biomedical applications, their scarce reproducibility, uncontrollable morphology, and broad size distributions render the limit of these materials in clinical applications. Furthermore, the potential toxicity of new Xene based nanodevices for medicinal use should always be considered and addressed before their approval by the regulatory authorities. Hence, more than ten key factors in defining the safety grade have been described by some authors to evaluate the potential toxicity of new nanomaterials. Nevertheless, the characteristics of Xenes could be changed during biological tests, which makes the physicochemical characterization of Xenes performed under the same experimental conditions more complex. Based on this, a regulation which contains some crucial factors to standardize the approach of comparing characterization and results should be proposed. Some efforts have been made towards this direction, and researchers have presented some minimal agreements for nanomaterial characterization including the synthesis process of materials and the biological test. In addition, although Xenes may have great advantages in terms of their easier mechanisms of metabolism and degradability in biological systems because of their simple elemental composition compared to other 2D materials (*e.g.*, TMDs, MXenes), the nano–bio interactions of Xenes that determine the fate of these materials in biosystems still remain largely unexplored. Our previous reports revealed that the majority of intravenously injected Xenes (*e.g.*, antimonene) accumulated in livers compared to other organs, while most of the materials can be cleared *via* excretion after one week.[6,7] However, more systematic studies are still needed to shed light on the possible accumulation *in vivo* and induced resorption or excretion of these Xenes with minimal side effects. As can be observed in Table 1, although the biomedical applications of some Xenes (*e.g.*, phosphorene) have been widely explored,[5] some newly synthesized Xenes are still at the beginning for their bio-applications (*e.g.*, gallenene, germanene, stanene, arsenene, and selenene), which means that in the near future these Xenes will find more opportunities.

In regard to Xenes, some physicochemical characteristics including the number of layers, the degree of oxidation, and the lateral dimension must be considered in material characterization. However, the differences in biological behaviour between single-, few and multi-layer sheets, and small and large sheets of Xenes have still no clear definition, while the oxidation degree of Xenes can also evoke negative effects. Moreover, easy aggregation, fast degradation, and insufficient stability also limited the application of Xenes in biological environments, which should be further resolved. It should also be noted that the factor of Xenes' degradation has two sides: too fast degradation will limit the therapeutic effect of developed Xenes, while their degradability is preferred in biomedical applications. Therefore, it is also important to prepare functionalized Xenes with adjustable

degradation rates for both the best therapeutic efficacy and the lowest systemic toxicity. For Xenes, their initial structural characteristics in dispersions are certainly not the same after several hours or even a day or more, so it is very important to figure out the change in suspension and apply this to physiological experiments. Therefore, the dispersion and stability of Xenes' aqueous solutions are the first priority for biological experiments, and improving their dispersity and stability is critical for advancing in different biomedical applications. Tremendous methods have also been exploited to modify Xenes to obtain stable sheets in suspensions for biomedical applications. Regardless of the inherent biocompatibility of Xenes, their dispersion should be precisely quantified to minimize possible biological effects for further understanding their true role.

Based on the above considerations, comprehending the physicochemical parameters of Xenes will be a guiding platform for the development of new biocompatible Xenes in biomedicinal applications. According to previous reports and standardized data, we could better compare the differences of Xene based sheets, and clearly understand the relationships between their structures and respective characteristics. This will advance the development of prediction models and broaden the knowledge about relationships between the nanosheets and biological tissue, and hence clear the way of Xenes for clinic trials. Although extensive theoretical calculation and experimental research about the characterization of Xenes are underway, their journey for successful clinical application is still very long and tortuous. For instance, surface modifications and particle size play pivotal roles in modulating the biological behaviours of Xenes, but it is necessary to study the systemic cytotoxicity (both short-term and long-term), transport pathways and biological immunity of different Xenes with different sizes and modifications. A further and deeper exploration of Xene knowledge and clinical transformation require the joint efforts from scientific researchers of interdisciplinary and industrial sectors. We expect that the development of nanotechnology will promote more fundamental and technological breakthroughs to afford the limitless application of Xenes in various biomedical fields in the near future.

Conflicts of interest

The authors declare the following competing financial interest(s): O. C. F. has financial interests in Selecta Biosciences, Tarveda Therapeutics, Placon Therapeutics, and Seer.

Acknowledgements

This work was supported by a U.S. METAvivor Early Career Investigator Award (Grant No. 2018A020560, W. T.), Harvard Medical School (HMS)/Brigham and Women's Hospital (BWH) Department of Anesthesiology – Basic Scientist Grant (Grant No. 2420 BPA075, W. T.) and CRI project (Grant No. 2018R1A3B1052702, J. S. K.).

Notes and references

1 G. Reina, J. M. Gonzalez-Dominguez, A. Criado, E. Vazquez, A. Bianco and M. Prato, *Chem. Soc. Rev.*, 2017, **46**, 4400–4416.
2 X. Kong, Q. Liu, C. Zhang, Z. Peng and Q. Chen, *Chem. Soc. Rev.*, 2017, **46**, 2127–2157.
3 A. Molle, J. Goldberger, M. Houssa, Y. Xu, S. C. Zhang and D. Akinwande, *Nat. Mater.*, 2017, **16**, 163–169.
4 A. J. Mannix, Z. Zhang, N. P. Guisinger, B. I. Yakobson and M. C. Hersam, *Nat. Nanotechnol.*, 2018, **13**, 444–450.
5 M. Qiu, W. X. Ren, T. Jeong, M. Won, G. Y. Park, D. K. Sang, L. P. Liu, H. Zhang and J. S. Kim, *Chem. Soc. Rev.*, 2018, **47**, 5588–5601.
6 W. Tao, X. Ji, X. Zhu, L. Li, J. Wang, Y. Zhang, P. E. Saw, W. Li, N. Kong, M. A. Islam, T. Gan, X. Zeng, H. Zhang, M. Mahmoudi, G. J. Tearney and O. C. Farokhzad, *Adv. Mater.*, 2018, **30**, 1802061.
7 W. Tao, X. Y. Ji, X. D. Xu, M. A. Islam, Z. J. Li, S. Chen, P. E. Saw, H. Zhang, Z. Bharwani, Z. L. Guo, J. J. Shi and O. C. Farokhzad, *Angew. Chem., Int. Ed.*, 2017, **56**, 11896–11900.
8 P. P. Lei, R. An, P. Zhang, S. Yao, S. Y. Song, L. L. Dong, X. Xu, K. M. Du, J. Feng and H. J. Zhang, *Adv. Funct. Mater.*, 2017, **27**, 1702018.
9 X. T. Meng, X. H. Wang, Z. C. Cheng, N. Tian, M. C. Lang, W. J. Yan, D. M. Liu, Y. Z. Zhang and P. Wang, *ACS Appl. Mater. Interfaces*, 2018, **10**, 31136–31145.
10 W. Tao, X. Zhu, X. Yu, X. Zeng, Q. Xiao, X. Zhang, X. Ji, X. Wang, J. Shi, H. Zhang and L. Mei, *Adv. Mater.*, 2017, **29**, 1603276.
11 Y. Lin, Y. Wu, R. Wang, G. Tao, P. F. Luo, X. Lin, G. Huang, J. Li and H. H. Yang, *Chem. Commun.*, 2018, **54**, 8579–8582.
12 T. Y. Xue, W. Y. Liang, Y. W. Li, Y. H. Sun, Y. J. Xiang, Y. P. Zhang, Z. G. Dai, Y. H. Duo, L. M. Wu, K. Qi, B. N. Shiyananju, L. J. Zhang, X. Q. Cui, H. Zhang and Q. L. Bao, *Nat. Commun.*, 2019, **10**, 28.
13 S. Zhang, S. Guo, Z. Chen, Y. Wang, H. Gao, J. Gomez-Herrero, P. Ares, F. Zamora, Z. Zhu and H. Zeng, *Chem. Soc. Rev.*, 2018, **47**, 982–1021.
14 X. Ji, N. Kong, J. Wang, W. Li, Y. Xiao, S. T. Gan, Y. Zhang, Y. Li, X. Song, Q. Xiong, S. Shi, Z. Li, W. Tao, H. Zhang, L. Mei and J. Shi, *Adv. Mater.*, 2018, e1803031.
15 A. J. Mannix, B. Kiraly, M. C. Hersam and N. P. Guisinger, *Nat. Rev. Chem.*, 2017, **1**, 0014.
16 B. E. Douglas and S.-M. Ho, *Structure and chemistry of crystalline solids*, Springer, New York, 2006.
17 A. R. Oganov, J. Chen, C. Gatti, Y. Ma, Y. Ma, C. W. Glass, Z. Liu, T. Yu, O. O. Kurakevych and V. L. Solozhenko, *Nature*, 2009, **457**, 863.
18 V. Kochat, A. Samanta, Y. Zhang, S. Bhowmick, P. Manimunda, S. A. S. Asif, A. S. Stender, R. Vajtai, A. K. Singh, C. S. Tiwary and P. M. Ajayan, *Sci. Adv.*, 2018, **4**, e1701373.
19 Y. Xing, H. M. Zhang, H. L. Fu, H. Liu, Y. Sun, J. P. Peng, F. Wang, X. Lin, X. C. Ma, Q. K. Xue, J. Wang and X. C. Xie, *Science*, 2015, **350**, 542–545.
20 A. Bansil, H. Lin and T. Das, *Rev. Mod. Phys.*, 2016, **88**, 021004.

21 L. Tao, E. Cinquanta, D. Chiappe, C. Grazianetti, M. Fanciulli, M. Dubey, A. Molle and D. Akinwande, *Nat. Nanotechnol.*, 2015, **10**, 227.
22 M. R. Tchalala, M. A. Ali, H. Enriquez, A. Kara, A. Lachgar, S. Yagoubi, E. Foy, E. Vega, A. Bendounan, M. G. Silly, F. Sirotti, S. Nitshe, D. Chaudanson, H. Jamgotchian, B. Aufray, A. J. Mayne, G. Dujardin and H. Oughaddou, *J. Phys.: Condens. Matter*, 2013, **25**, 442001.
23 E. Bianco, S. Butler, S. Jiang, O. D. Restrepo, W. Windl and J. E. Goldberger, *ACS Nano*, 2013, **7**, 4414–4421.
24 F. F. Zhu, W. J. Chen, Y. Xu, C. L. Gao, D. D. Guan, C. H. Liu, D. Qian, S. C. Zhang and J. F. Jia, *Nat. Mater.*, 2015, **14**, 1020–1025.
25 S. Lin, Y. Chui, Y. Li and S. P. Lau, *FlatChem*, 2017, **2**, 15–37.
26 M. Qiu, D. Wang, W. Liang, L. Liu, Y. Zhang, X. Chen, D. K. Sang, C. Xing, Z. Li, B. Dong, F. Xing, D. Fan, S. Bao, H. Zhang and Y. Cao, *Proc. Natl. Acad. Sci. U. S. A.*, 2018, **115**, 501–506.
27 R. Gusmão, Z. Sofer, D. Bouša and M. Pumera, *Angew. Chem., Int. Ed.*, 2017, **56**, 14417–14422.
28 J. Ji, X. Song, J. Liu, Z. Yan, C. Huo, S. Zhang, M. Su, L. Liao, W. Wang, Z. Ni, Y. Hao and H. Zeng, *Nat. Commun.*, 2016, **7**, 13352.
29 S.-C. Chen, J.-Y. Wu and M.-F. Lin, *New J. Phys.*, 2018, **20**, 062001.
30 T. Tono, T. Hirahara and S. Hasegawa, *New J. Phys.*, 2013, **15**, 105018.
31 Q.-Q. Yang, R.-T. Liu, C. Huang, Y.-F. Huang, L.-F. Gao, B. Sun, Z.-P. Huang, L. Zhang, C.-X. Hu, Z.-Q. Zhang, C.-L. Sun, Q. Wang, Y.-L. Tang and H.-L. Zhang, *Nanoscale*, 2018, **10**, 21106–21115.
32 L. Xian, A. Pérez Paz, E. Bianco, P. M. Ajayan and A. Rubio, *2D Mater.*, 2017, **4**, 041003.
33 J. Qin, G. Qiu, J. Jian, H. Zhou, L. Yang, A. Charnas, D. Y. Zemlyanov, C. Y. Xu, X. Xu, W. Wu, H. Wang and P. D. Ye, *ACS Nano*, 2017, **11**, 10222–10229.
34 Y. Wang, G. Qiu, R. Wang, S. Huang, Q. Wang, Y. Liu, Y. Du, W. A. Goddard, M. J. Kim, X. Xu, P. D. Ye and W. Wu, *Nat. Electron.*, 2018, **1**, 228–236.
35 Q. Wang, M. Safdar, K. Xu, M. Mirza, Z. Wang and J. He, *ACS Nano*, 2014, **8**, 7497–7505.
36 J. D. Shao, H. H. Xie, H. Huang, Z. B. Li, Z. B. Sun, Y. H. Xu, Q. L. Xiao, X. F. Yu, Y. T. Zhao, H. Zhang, H. Y. Wang and P. K. Chu, *Nat. Commun.*, 2016, **7**, 12967.
37 J. R. Choi, K. W. Yong, J. Y. Choi, A. Nilghaz, Y. Lin, J. Xu and X. N. Lu, *Theranostics*, 2018, **8**, 1005–1026.
38 J. J. Zhao, H. S. Liu, Z. M. Yu, R. G. Quhe, S. Zhou, Y. Y. Wang, C. C. Liu, H. X. Zhong, N. N. Han, J. Lu, Y. G. Yao and K. H. Wu, *Prog. Mater. Sci.*, 2016, **83**, 24–151.
39 R. G. Quhe, R. X. Fei, Q. H. Liu, J. X. Zheng, H. Li, C. Y. Xu, Z. Y. Ni, Y. Y. Wang, D. P. Yu, Z. X. Gao and J. Lu, *Sci. Rep.*, 2012, **2**, 853.
40 X. Zeng, M. Luo, G. Liu, X. Wang, W. Tao, Y. Lin, X. Ji, L. Nie and L. Mei, *Adv. Sci.*, 2018, **5**, 1800510.
41 S. Kaneko, H. Tsuchiya, Y. Kamakura, N. Mori and M. Ogawa, *Appl. Phys. Express*, 2014, **7**, 035102.
42 R. G. Amorim and R. H. Scheicher, *Nanotechnology*, 2015, **26**, 154002.
43 D. C. C. Mayorga-Martinez, D. R. Gusmão, P. D. Z. Sofer and P. D. M. Pumera, *Angew. Chem., Int. Ed.*, 2019, **58**, 134–138.
44 X. Chen, Y. Wu, Z. Wu, Y. Han, S. Xu, L. Wang, W. Ye, T. Han, Y. He, Y. Cai and N. Wang, *Nat. Commun.*, 2015, **6**, 7315.
45 X. Yu, A. Li, C. Zhao, K. Yang, X. Chen and W. Li, *ACS Nano*, 2017, **11**, 3990–4001.
46 C. Sun, L. Wen, J. Zeng, Y. Wang, Q. Sun, L. Deng, C. Zhao and Z. Li, *Biomaterials*, 2016, **91**, 81–89.
47 X. Zhu, X. Ji, N. Kong, Y. Chen, M. Mahmoudi, X. Xu, L. Ding, W. Tao, T. Cai, Y. Li, T. Gan, A. Barrett, Z. Bharwani, H. Chen and O. C. Farokhzad, *ACS Nano*, 2018, **12**, 2922–2938.
48 H. U. Lee, S. Y. Park, S. C. Lee, S. Choi, S. Seo, H. Kim, J. Won, K. Choi, K. S. Kang, H. G. Park, H. S. Kim, H. R. An, K. H. Jeong, Y. C. Lee and J. Lee, *Small*, 2016, **12**, 214–219.
49 W. Chen, J. Ouyang, H. Liu, M. Chen, K. Zeng, J. Sheng, Z. Liu, Y. Han, L. Wang, J. Li, L. Deng, Y. N. Liu and S. Guo, *Adv. Mater.*, 2017, **29**, 1603864.
50 T. Yang, H. Ke, Q. Wang, Y. A. Tang, Y. Deng, H. Yang, X. Yang, P. Yang, D. Ling, C. Chen, Y. Zhao, H. Wu and H. Chen, *ACS Nano*, 2017, **11**, 10012–10024.
51 H. Wang, X. Yang, W. Shao, S. Chen, J. Xie, X. Zhang, J. Wang and Y. Xie, *J. Am. Chem. Soc.*, 2015, **137**, 11376–11382.
52 T. Guo, Y. Wu, Y. Lin, X. Xu, H. Lian, G. Huang, J.-Z. Liu, X. Wu and H.-H. Yang, *Small*, 2018, **14**, 1702815.
53 H. Huang, L. He, W. Zhou, G. Qu, J. Wang, N. Yang, J. Gao, T. Chen, P. K. Chu and X.-F. Yu, *Biomaterials*, 2018, **171**, 12–22.
54 J. Ouyang, R.-Y. Liu, W. Chen, Z. Liu, Q. Xu, K. Zeng, L. Deng, L. Shen and Y.-N. Liu, *J. Mater. Chem. B*, 2018, **6**, 6302–6310.
55 W. Chen, J. Ouyang, X. Yi, Y. Xu, C. Niu, W. Zhang, L. Wang, J. Sheng, L. Deng, Y.-N. Liu and S. Guo, *Adv. Mater.*, 2018, **30**, 1703458.
56 B. Yang, J. Yin, Y. Chen, S. Pan, H. Yao, Y. Gao and J. Shi, *Adv. Mater.*, 2018, **30**, 1705611.

